

Microfluidic Synthesis of Luminescent and Plasmonic Nanoparticles: Fast, Efficient, and Data-Rich

Julia Nette, Philip D. Howes,* and Andrew J. deMello*

Microfluidic approaches to nanomaterial synthesis provide an effective means of making high quality products, with exquisite control over electronic, optical, and structural properties. Furthermore, microfluidic reactors integrating analytics and real-time reaction control have recently emerged as powerful tools in automating materials exploration and reaction parameter mapping, with a rapidity and efficiency that is inaccessible to traditional flask-based methods. Herein, the recent innovations in the microfluidic synthesis of photonic nanoparticles, whose varied luminescent and plasmonic properties have found great application in the biomedical and optoelectronic sciences, are presented. Special attention is placed on the achievements and promise of microfluidic approaches in automated multidimensional reaction parameter screening employing *in situ* optical characterization. In an extended outlook, the future of the field is explored, looking toward the integration of smart control systems and machine learning algorithms, and demonstrating how maximal positive impact can be achieved. Far from degrading or replacing the ingenuity of the experimentalist, these tools will provide new powers of exploration, augmenting the discovery process. Further, through automation and miniaturization, it is expected that such approaches will fulfill the moral imperative of maximizing the benefit derived from the natural resources consumed in conducting research.

1. Introduction

Nanoscience describes the manipulation of matter on the nanoscale, with a view to building novel functional (nano) systems or uncovering new phenomena of fundamental and practical importance. In simple terms, a nanomaterial may be defined as any structure that has at least one dimension of a size below 1 μm (but typically below 100 nm), while a nanoparticle has the same size constraint in three dimensions.^[1] On such scales, many materials exhibit new and interesting phenomena, forming a unique set of size-dependent properties.^[1,2] This is particularly significant for photonic nanoparticles, a term we use here to refer to any nanoparticles whose dominant

functionality arises due to the interaction with and/or generation of light.

The field of photonic nanoparticles is wide in its variety of composition, morphology, size, and property (Figure 1). Nanoparticles whose most beneficial optical characteristics stem from their photoluminescence (PL) include inorganic and organic semiconductor, organic dye-based and semiconductor perovskite nanoparticles, and noble metal nanoclusters.^[3] In contrast, the dominant functionality of noble metal nanoparticles arises due to their ability to form surface plasmons.^[4] Together, such nanoparticles have been the focus of a tremendous amount of attention over the past three decades, with a myriad of potential applications including optical and biological sensing,^[5–7] medical imaging and drug delivery,^[8,9] photoacoustic imaging,^[10,11] photothermal therapy,^[12] light-emitting diodes (LEDs),^[13,14] and photovoltaics.^[15]

Beyond the obvious dependence on elemental composition, the properties of most photonic nanoparticles are highly dependent on their size, shape, and surface character.^[16] For example, the emission of

compound semiconductor quantum dots (QDs) is strongly coupled to the particle diameter, while the plasmonic peak of noble metal nanoparticles varies dramatically as a function of nanoparticle shape. Such relationships mean that the ultimate properties of nanoparticles are acutely sensitive to the reaction conditions used during their synthesis. Accordingly, the ability to exert a tight control over the synthesis provides a route to ensuring in-batch and batch-to-batch product consistency. Unfortunately, such control is exceptionally difficult to achieve when using traditional flask-based techniques (especially for rapid reactions), due to an inability to control heat and mass transport in a rapid manner.^[17]

In recent years, microfluidic reactors have emerged as outstanding tools for synthesizing a wide range of photonic nanoparticles, providing for exquisite control over particle size, particle size distributions, and batch-to-batch reproducibility.^[18] The superior heat- and mass-transfer rates representative of such environments, allow for dramatic reductions in mixing timescales and guarantee uniform temperatures across the entirety of the reaction volume. Additionally, microfluidic platforms can be configured so as to isolate different steps within complex reaction schemes and thus exert even finer control over the synthetic process.

J. Nette, Dr. P. D. Howes, Prof. A. J. deMello
Institute for Chemical and Bioengineering
Department of Chemistry and Applied Biosciences
ETH Zürich

Vladimir Prelog Weg 1, Zürich 8093, Switzerland
E-mail: philip.howes@chem.ethz.ch; andrew.demello@chem.ethz.ch

 The ORCID identification number(s) for the author(s) of this article can be found under <https://doi.org/10.1002/admt.202000060>.

DOI: 10.1002/admt.202000060

Continuous- and segmented-flow reactors have been used to synthesize a wide range of nanomaterials. Continuous-flow formats offer a high degree of synthetic flexibility, are tolerant to variations in flow rates and solvents, and facilitate multistep processing using simple fluid circuits. That said, continuous flow reactors are limited by issues related to Taylor dispersion, solute–surface interactions, cross-contamination, and the need for extended channel lengths. Fortunately, segmented-flow or droplet-based reactors elegantly overcome many of these drawbacks. In droplet flows, reaction volumes contained in the discrete phase are isolated from channel surfaces by the carrier fluid (preventing solute–surface interactions) and if large enough to fill the channel cross-section, move at a constant linear velocity (thus removing residence time distributions).^[19–21]

Although the inherent advantages of microfluidic reactors in photonic nanoparticle synthesis are of key importance, they are not the primary focus of the current review. Herein, we are more interested in assessing the prospects of automated microfluidic reactors in conducting rapid, efficient, and data-rich materials exploration and reaction optimization via multidimensional parameter screening. Such approaches essentially split synthesis parameter space into separate variables that can be controlled in an automated fashion, through the variation of input stream flow rates, reaction temperature, and residence time. Subsequently, integrated analytics (e.g., extracting photoluminescence and absorption data) are used to analyze products in real time, either logging data as part of a preprogrammed parameter scan, or feeding it back into an automated reaction controller to tune synthesis variables toward a desired product. Accordingly, we see that this technology set necessitates advances in system automation, machine learning, and analytics integration. Put simply, by combining the key advantages of miniaturization and automation, dramatic gains in both resource and time efficiency can be made. We believe this generic approach will rapidly accelerate the optimization of existing photonic nanoparticles, and open new avenues to enhanced formulation complexities that cannot be effectively explored using traditional flask-based approaches.

Herein, we first provide a general overview of microfluidic tools for the synthesis of nanoparticles, and follow this by an assessment of studies where microfluidic systems have been used for multidimensional parameter screening. Subsequently, we discuss how system automation is beginning to revolutionize our abilities to perform fast and efficient reaction parameter optimization, discover new particle formulations, optimize reaction conditions, and perform targeted synthesis. Finally, we conclude with a discussion of some of the wider challenges and opportunities in the field.

2. Methods in Microfluidics and Optical Characterization

2.1. Nanoparticle Synthesis in Microfluidic Environments

The sensitivity of nanoparticle properties to their size, shape, and surface effects necessitates a high level of control and reproducibility in their synthesis.^[22] This is exceptionally



Julia Nette is a Ph.D. student in the deMello group at ETH Zürich, having started in 2018. She completed her bachelor and master studies in nanoscience at the University of Hamburg in 2018, during which she completed a research secondment to the University of California, Berkeley. Her current research focuses on the microfluidic synthesis and characterization of nanoparticles, in particular fluorescent nanoparticles.



Philip D. Howes is a senior scientist in the deMello group at ETH Zürich. He moved to ETH in 2017 with an individual Marie Skłodowska Curie Fellowship, having previously completed a post-doctoral position at Imperial College London, and a Ph.D. at King's College London. His research focuses on the synthesis, functionalization, and characterization of luminescent and plasmonic nanoparticles, for applications in biomedicine and optoelectronics.



Andrew J. deMello is a professor of Biochemical Engineering in the Department of Chemistry and Applied Biosciences at ETH Zürich and Head of the Institute for Chemical and Bioengineering. Previously, he was a professor of Chemical Nanosciences in the Chemistry Department at Imperial College London. His group's research interests cover a broad range of activities in the general area of microfluidics and nanoscale science. Primary specializations include the development of microfluidic devices for high-throughput biological and chemical analysis, ultrasensitive optical detection techniques, imaging flow cytometry, novel methods for nanoparticle synthesis, the exploitation of semiconducting materials in diagnostic applications, and the development of intelligent microfluidic systems.

difficult to achieve via classical flask-based methods,^[23] where small (but inevitable) variations in reaction conditions (such as temperature, precursor concentration, ligands, and solvent

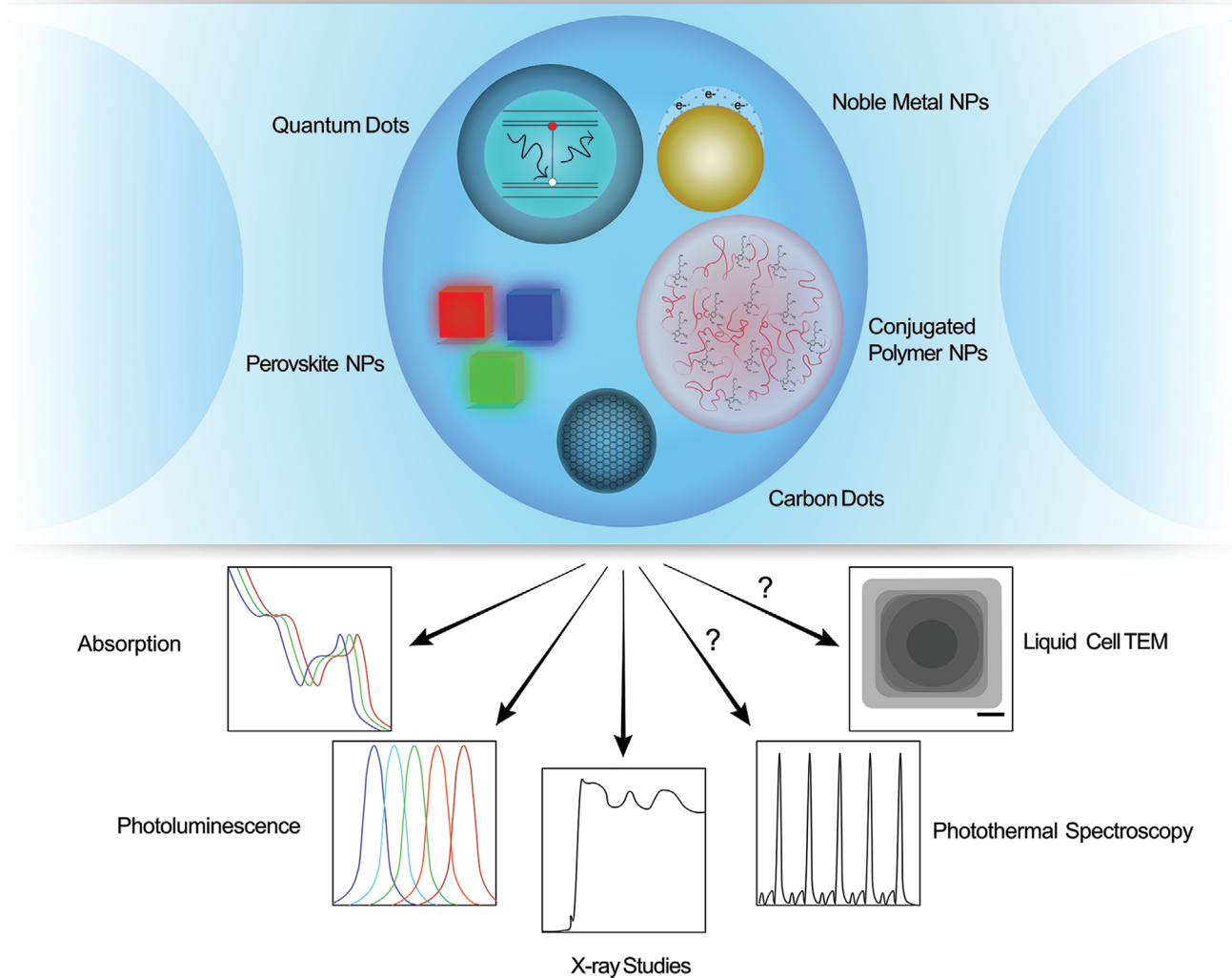


Figure 1. Schematic of the various photonic nanoparticles discussed in this review, and the optical detection methods that can be used to characterize them.

composition) yield dramatic shifts in product properties.^[24] Product inconsistencies in flask-based synthesis arise both in-batch (through high polydispersities) and between batches.^[25] In contrast, the reduced reaction volumes typical in microfluidic environments allow for greatly improved heat- and mass-transfer, leading to higher reaction yields, reduced product dispersities,^[26] and higher quality nanoparticles.^[20,22,27]

Synthetic approaches in microfluidics vary with regard to flow scheme and device material. Two generic flow schemes are commonly encountered in microfluidic systems, namely, single-phase continuous flow and two-phase segmented (or “droplet”) flow (Figure 2). Continuous flow schemes (Figure 2a) involve the motivation of a single fluid phase along a microfluidic flow path. As noted, such an approach can be used for complex, multistep processes, but is limited by the parabolic nature of the flow, which results in wide residence time distributions and a propensity for reactor fouling. In continuous flow schemes, mixing typically occurs through diffusion (Figure 2c) at Reynolds numbers (Re) below 2000.^[29] In contrast, segmented

flows involve a liquid–liquid or gas–liquid flow, and are most normally characterized by a series of spatially separated reaction volumes forming an “ordered emulsion” (with encapsulated volumes typically on the fL–nL scale).^[28] In a gas–liquid segmented flow, elongated volumes of gas spatially separate liquid droplet reaction volumes. A liquid–liquid segmented flow (Figure 2b) describes the scenario where a carrier fluid (continuous phase) physically separates distinct volumes (droplets) of an immiscible discrete phase. If the formed droplets are smaller than the cross-section dimensions of the containing channel, they will form spheres. Otherwise they will conform to the shape of the channel, and for example form elongated allantoid droplets. It is important to note that clean transport of droplet contents is ensured if the continuous phase is chosen so as to preferentially wet the channel surface. If such a condition is fulfilled, the discrete phase will remain separated from the channel surface by a thin layer of the carrier fluid.^[29] Segmented flows are especially useful when performing reactive processes, and overcome mixing restrictions associated with continuous flows due to

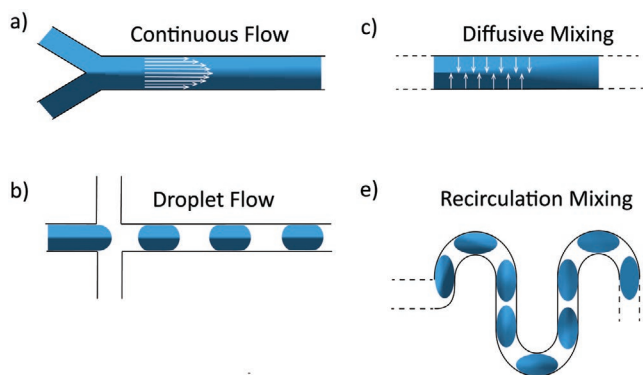


Figure 2. Flow patterns in microfluidic channels: a) single-phase continuous flow with parabolic flow profile, b) two-phase segmented/droplet flow, c) single-phase continuous flow with diffusive mixing, and d) two-phase segmented/droplet flow in serpentine mixing channels.

negligible residence time distributions and the passive generation of chaotic advection in winding channels (Figure 2d).^[23,29,30] In addition, segmented flows allow for precise temporal control over unit operations (such as reaction initiation or reagent addition) and the separation of multiple process steps through droplet merging, splitting, sorting, and picoinjection.^[30,31] Multiphase microfluidic flows are not necessarily limited to a two-phase system, for example, Duraiswamy and Khan demonstrated microfluidic composite foams with an aqueous liquid and a gas phase immersed in an oil phase for the synthesis of gold “nanoshells” and “nanoislands” on silica nanoparticle surfaces. This three-phase flow evidently overcomes liquid–liquid segmented flow limitations through residue prevention at the junction and hindrance of droplet fusion.^[32]

In addition to the distinction between flow formats, microfluidic reactors can be categorized as being either capillary-based or chip-based. Capillary reactors are most commonly made from commercially available plastic tubing with high chemical and temperature stability (such as polytetrafluoroethylene (PTFE) and fluorinated ethylene propylene (FEP)) or glass capillaries, and offer a relatively simple way to construct sophisticated flow systems.^[23,33,34] However, chip-based reactors are far richer in respect to their structure, geometry, and material choice. Chips can be made from many materials, including glass, silicon,^[35] elastomers,^[36] plastics,^[37] ceramics,^[38] and metals.^[39] Within the broad field of “microfluidics” the most

popular chip material is poly(dimethylsiloxane) (PDMS).^[40] That said, its poor solvent and thermal compatibility severely limits its use in most nanoparticle synthesis applications. It is possible to coat PDMS channels with more robust materials like PTFE,^[41,42] but this is a relatively specialized process and not recommended when operating under harsh reaction conditions. To conclude, while the chip-based approach excels in controlling system complexity, variability, and flexibility,^[35,43,44] it is far more involved than the capillary approach.

In continuous flow reactors, reagent streams are combined at a junction. These can be simple in structure (e.g., a T-junction), or they can be more complex, incorporating hydrodynamic flow focusing structures, where an inner stream is introduced between outer coflows (2D) or coaxially inside an outer flow (3D focusing). Such coflows surround and focus the inner flow into a thin stream.^[18,45] In a laminar flow regime, mixing between the fluids occurs solely via diffusion. In an attempt to overcome the limitations of diffusion-based mixing, transitional jet-based mixers, where a coflowing outer fluid generates microvortices surrounding an inner jet have been investigated.^[46] In the example shown in Figure 3a, the sequential nanoprecipitation of a nanoparticle core and shell at <5 ms mixing time and good batch-to-batch reproducibility allowed for the synthesis of nanoparticles with a polydispersity index (PDI) below 0.2 at $Re > 10$, and high drug loading degrees above 40% (compared to above 5% drug loading in particles synthesized via single nanoprecipitation).^[46] In contrast, diffusive mixing in segmented flows can be dramatically accelerated by conveying the droplets through serpentine channels, which induce internal circulation and chaotic advection within the liquid segments.^[29] This is a significant advantage of segmented flow microfluidic platforms.

For the synthesis of inorganic nanocrystals, reagents are typically chemically bound in precursors of each component, and react to form the desired nanoparticles (Figure 3b). In such systems, the rate of mixing of precursors and solvents is not always a reaction limiting step, so there may be some flexibility in the requirements of superfast mixing. This is especially present in cases where the reaction is initiated by temperature, as a time delay between mixing and heating can be introduced to ensure complete mixing before the reaction starts. An illustrative example is shown in Figure 3b, where core and shell synthesis of InP/ZnSe nanoparticles proceeds in a two-step continuous flow reactor with integrated heating and cooling units and an inline mixer.^[47]

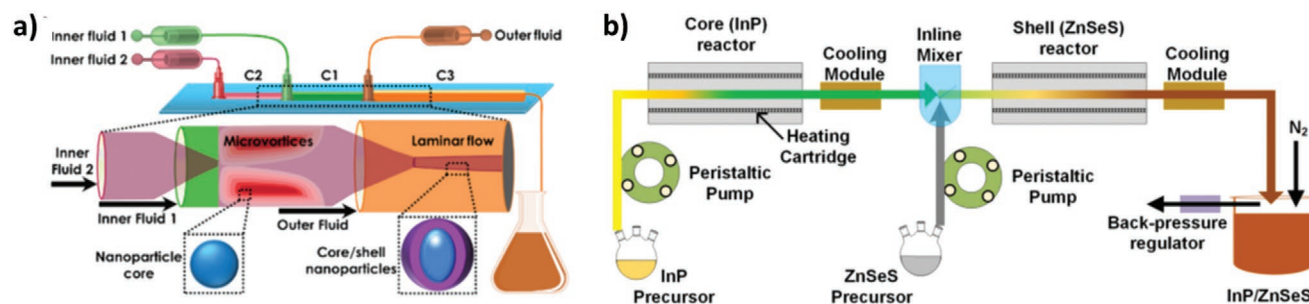


Figure 3. Nanoparticle synthesis in microfluidic systems: a) polymeric core–shell composites from nanoprecipitation in flow. Reproduced with permission.^[46] Copyright 2017, American Chemical Society. b) A millifluidic reactor for multistep-synthesis of InP/ZnSe particles with two stages, cooling modules, and a peristaltic pump system. b) Reproduced with permission.^[47] Copyright 2018, Wiley-VCH.

For the synthesis of organic nanoparticles, reprecipitation (or nanoprecipitation) is the most commonly used approach, where a solution containing the nanoparticle precursor material in a good solvent is rapidly injected into a miscible poor solvent, resulting in rapid aggregation of the material into solid nanoparticles.^[48] In contrast to the synthesis of inorganic nanoparticles, here mixing is the nucleation-limiting step, therefore the ability to realize rapid mixing is of utmost importance.^[49,50] Since organic nanoparticle production is usually conducted in continuous flows (due to its relative simplicity), with reagents dissolved in an organic solvent, these syntheses are most easily performed using capillary-based systems.^[33] For example, Figure 3a shows a two-stage continuous-flow nanoprecipitation platform for the core and shell synthesis of polymer composite nanoparticles, demonstrating the use of microvortices for rapid mixing (<0.5 ms) and two stage core/shell formation.^[46] Here, we have only provided a cursory overview of nanoparticle synthesis within microfluidic reactors. Interested readers can find excellent and detailed reviews on this topic elsewhere.^[20,23,24,51]

2.2. Optical Characterization Methods

While the inherent advantages of the microfluidic approach in synthesizing high quality nanoparticles are noteworthy, the true power of these systems is only unleashed on integration of analytical tools able to probe reaction products in situ, during and after particle formation. Such facility opens the door to the design and implementation of multidimensional parameter screening and reaction kinetics analysis. Optical detection methods are ideal for such a purpose as they do not interfere with the reaction, and are rapid and highly sensitive, facilitating real-time analysis of the sample. Optical methods most commonly assess the scattering, absorption or emission properties of the sample,^[52] which in the case of photonic nanoparticles, tend to be strong optical effects that are well-suited for product monitoring. We now provide a brief overview of the optical characterization methods pertinent to in situ analysis and monitoring of photonic nanoparticles in microfluidic reactors.

2.2.1. Photoluminescence and Absorption Spectroscopy

Absorption and PL detection are quantitative tools that in many circumstances allow the characterization of nanoparticle size, population size distribution, shape, surface integrity and composition.^[39] The advantages associated with optical measurement techniques are numerous and include their ease of use, high sensitivity, low (mass and concentration) limits of detection, noninvasiveness, and fast response time.^[7] Although, both absorption and PL measurements can be used for quantitative analysis of nanoparticle populations, with spectral features providing information about electronic structure, nanoparticle size and population size distributions,^[53,54] absorption measurements are often compromised due to the fact that optical pathlengths in microfluidic systems are by definition small. That said, PL and absorption detection can be easily

integrated with both capillary-based and chip-based reactors (using free-space or integrated optical components^[21]) to ensure real-time product analysis on sub-millisecond timescales.^[21,39,55]

2.2.2. X-Ray Studies

X-ray spectroscopic measurements can yield superior quantitative information on the crystal and electronic structure of nanoparticles compared to conventional optical detection methods, and thus they have been applied to excellent effect in microfluidic systems, as we discuss later. However, the complexity of the measurement process can be a considerable challenge.^[21,56] X-ray studies encompass a number of distinct yet complementary methods. For example, in X-ray absorption spectroscopy (XAS), photons are used to excite inner electrons, yielding spectra consisting of regions corresponding to the X-ray absorption near edge structure (XANES)^[57,58] and extended X-ray absorption fine structure (EXAFS).^[59] XAS measurements provide for the analysis of electronic structure in specific oxidation states, coordination and crystal structure in local order and surface condition, with a time resolution between 1 and 100 ms.^[57,60] The power of XAS lies in the fact that every element has a different spectrum, which makes the technique sensitive to the elemental composition of the nanoparticle.^[55] Conversely, both EXAFS and XANES provide information on the immediate surroundings of absorbing species. EXAFS is sensitive to the elemental composition and disorder, while XANES probes the electronic states of absorbing species. That said, although EXAFS is a potent technique for structural elucidation, it is sensitive to artifacts, with interpretation often being difficult.^[61] Finally, small angle X-ray scattering (SAXS) is used to elucidate the morphology of a system, and has been used to study the nucleation and growth mechanisms of nanocrystals.^[57,62]

3. Toward Multidimensional Parameter Screening

We now discuss the evolution of microfluidic tools for nanoparticle synthesis classified by material type. A key feature of this analysis is an assessment of the status of and potential for automated multidimensional parameter screening.

3.1. Generalized System Overview

Microfluidic systems for the synthesis and characterization of nanoparticles involve multiple and distinct operations linked in series, but with the option to readily add operations in parallel. Such an integrated system can be automated to coordinate each of its units, provide operational flexibility, and allow multidimensional parameter screening if desired. Furthermore, if a reactor is configured to perform real-time product optimization, then data originating from the in situ characterization channels (which can typically be incorporated at any point in the reaction time course) can be used to calculate new reaction parameters, for example, via dedicated algorithms.^[63]

Characterization of reaction products can be performed in situ and/or ex situ. Continuous characterization normally involves either direct measurements within the nucleation and growth channel (inline), or in a bypass or at the end of the channel (online). Conversely, discontinuous measurements are made away from the microfluidic platform, either through collection of aliquots during synthesis (atline), or collection of the entire product stream with postsynthesis characterization (offline).^[64] The form of the characterization unit depends on the physicochemical properties of the nanomaterials under investigation. Luminescent nanoparticles can be effectively probed using PL and absorption, while plasmonic nanoparticles are suited to analysis via absorbance, and when available, X-ray absorption and scattering.

3.2. Inorganic Semiconductor Nanoparticles

QDs are inorganic semiconductor nanocrystals that are size constrained in three dimensions. Such materials have received much attention due to their bright and size-tunable PL, high extinction coefficients, and excellent photostability. While their composition is variable, they are typically composed of elements of the II–VI, III–V, or IV–VI periodic groups (such as CdSe, CdS, ZnSe, CdxHg_{1-x}Te, InP, PbS, ZnO, and InAs). Among these, II–IV cadmium chalcogenides (CdX with X = S, Se, Te) are perhaps the most studied.^[65–67] Confinement in the regime of the material's Bohr radius limits exciton motion, leading to the quantum confinement effect (QCE), where the electronic bandgap varies as a function of particle diameter (with smaller particles yielding higher energy emission).^[2,7] A reduction in the size of inorganic nanoparticles is hence correlated with a blue shift in the absorption and PL. Accordingly, tuning the size and size distribution of a QD population affords direct control over optical properties. QDs have been extensively studied for both biomedical^[68,69] and optoelectronic applications.^[68,70] However, in biomedical applications and consumer electronics applications, the toxic heavy metal content of traditional QDs can be problematic. QD toxicity can arise due to leaking of heavy metal ions, for example, cadmium leakage from organic-capped CdSe QDs was observed after transfer to an aqueous environment (after at least 10 days).^[71] Further, the toxicity of oxidatively degraded PEG-5000-coated CdSe/ZnS QDs to developing zebrafish was analyzed by Wicinski et al.,^[72] who reported similar zebrafish mortality after exposure to degraded CdSe/ZnS compared to pure selenium nanoparticles and cadmium chloride. Further, the toxicity of chalcogenides, e.g., selenium compounds, is not negligible.^[73] While CdSe cores with intact ZnS or polymer shells are less toxic, it is challenging to ensure stability over longer periods of times.^[73,74] Thus, much research has focused on identifying less toxic alternatives. Examples include silicon-based QDs,^[7,75] lead-free perovskites,^[76,77] carbon dots (CDs),^[78] I–III–VI₂ chalcopyrite QDs such as CuInS₂ or CuInSe₂,^[75] and III–V QDs such as InP.^[79]

PL measurements are most frequently used for the characterization of nanoparticles due to their high sensitivities, short response times, low detection limits, and noninvasive character. Krishnadasan et al.^[80] were the first to report a microfluidic platform for the continuous flow synthesis of CdSe nanoparticles

with online PL detection. This system was used for a real-time kinetic study of the formation of CdSe QDs and its dependence on temperature, volumetric flow rates, and reaction time. In contrast, flow rate independent time scans were reported by Yao et al.,^[81] in a picoliter droplet microreactor for CdTe synthesis. Here, spectra were extracted at different positions along the reaction channel to provide for time resolution in kinetic studies. Such an approach involved relatively high flow rates (up to $\approx 30 \mu\text{L min}^{-1}$) and allowed inline study of different time points in the synthesis (instead of an end-point measurements), which effectively increased the accessible parameter space. Similarly, Sounart et al.^[82] studied the growth mechanism of cysteine-capped CdS QDs via spatially resolved PL imaging. Here, two precursors were mixed through diffusion in the laminar flow. Spatially resolved PL imaging revealed diffusion limited nucleation of CdS nanocrystals at the interface of the two streams, thus demonstrating spatially resolved growth of nanoparticles in a microfluidic reactor. An automated two-stage microfluidic reactor has been demonstrated by Pan et al.^[83] for the preparation of PbS nanoparticles with photovoltaic performance similar to bulk-synthesized particles. In this system, the optimized two-stage reactor allowed for precise temperature control and thus control over nucleation and growth, which enabled the synthesis of high-quality PbS nanoparticles.

In situ PL measurements are most commonly achieved using an LED or laser light source and spectrometer, with fiber optics delivering light into and out of the microfluidic environment. That said, there is a growing interest in the use of optically sectioned measurements. For example, Seibt et al.^[84] employed a double flow-focusing device for the synthesis of CdS nanoparticles (Figure 4a), and studied the reaction using confocal laser scanning microscopy (CLSM) (Figure 4b,c). Using a PL detection window of 410–650 nm, measurements were performed at different positions along the reaction channel, with flow rate variations being used to control detection times between 1 and 100 ms (Figure 4c). Importantly, these studies provided insight into the early stages of CdS nanocrystal formation, revealing that nucleation and growth kinetics strongly depend on flow-rates and device geometries, while particle size is primarily controlled by precursor concentration. Notably, the CLSM approach allows for extraction of a full PL image, as opposed to single spectral measurements in optical fiber detection schemes.

The concurrent use of PL and absorption spectroscopies can be used to build a comprehensive picture of the electronic and spectroscopic nature of target nanoparticles. Despite the fact that absorption measurements are somewhat harder to perform on small scales (due to reduced optical pathlengths), the basic approach can be used to good effect in photonic nanoparticle synthesis when product concentrations are high. For example, Toyota et al.^[34] reported the combinatorial synthesis of CdSe QDs using multiple parallel microreactors with coupled optical fibers for optical characterization. Temperature, reaction time, and additive concentration were varied, with the reaction being probed using both online absorption, and offline absorption and PL. Although the architecture required to integrate several microreactors is relatively complex, the basic method enabled the parallel study of multiple reactions, thus improving both throughput and sample consumption. In a similar manner, Kershaw et al.^[85] integrated online PL lifetime measurements

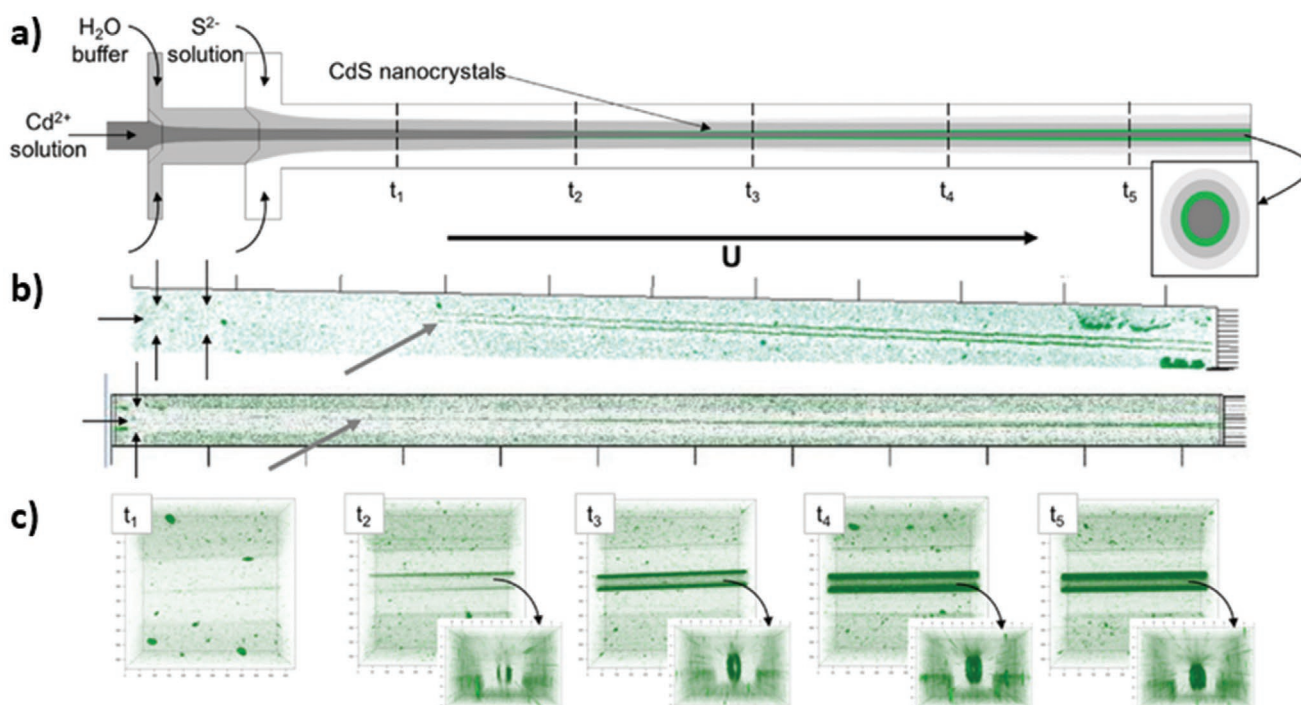


Figure 4. Microfluidic channel for flow focusing of a nanocrystal solution with a) a schematic of the channel with double flow focusing using an aqueous buffer between the reactants, b) a CLSM image of the channel with a gray arrow indicating the start of nucleation, and c) snapshots and cross-sectional CLSM images of the reaction solution. Reproduced with permission.^[84] Copyright 2019, Elsevier.

for the study of cation exchange reactions of Cd_xHg_{1-x}Te. In this system, a continuous blue shift of the absorption and PL spectra was observed during the cation exchange from Cd to Hg, with an initially fast and complex decay in PL, with increased multi-exponential character from CdTe to Cd_xHg_{1-x}Te. This observation was tentatively correlated to the biexponential decay of CdTe and triexponential decay of Hg compositions. It should be noted that PL lifetime analysis of nanoparticles currently lacks detailed interpretation, but the technique offers important insights into the electronic state of such systems. The approach reported by Kershaw et al. demonstrated the potential of a microfluidic platform with multiple optical detection methods, where the collection of both time-integrated and time-resolved data can yield huge data sets for analyzing growth kinetics and performing advanced parameter scanning.

In continuous flow systems, mixing of reactive species is normally achieved via (relatively slow) diffusive transport and defines the reaction limiting step. Minimizing the mixing time offers inherent advantages in respect to minimizing nanoparticle size dispersity, and for offering more accurate kinetic studies. The superior heat- and mass-transport associated with segmented flow provides for a much higher reproducibility in nanoparticle product properties, due to improved mixing and temperature uniformity in the contained droplet environment. Since temperature fluctuations as small as one or two degrees can have a notable effect on nanoparticle character,^[86] temperature uniformity is vital. Using a segmented flow approach in a tubing-based reactor, Abolhasani et al.^[87] introduced an oscillatory flow reactor for optical characterization of nanoparticle suspensions. Building on this attempt, Abolhasani et al.^[88]

studied the synthesis of CdSe and InP nanoparticles in single droplets using inline PL and absorption spectroscopy via optical fibers in a fully automated reactor. This single droplet, oscillatory approach allowed for the real-time characterization of one droplet over an extended time (up to 10 min), which is not limited by tubing length. This work showed the first in situ optical characterization of microfluidic CdSe/InP syntheses at elevated temperatures, up to 220 °C. Based on a population balance equation model from Rempel et al.^[89] and a preceding variation of this model from Maceiczky et al.,^[90] a theoretical model was proposed by Lazzari et al.^[91] to explain the evolution of the size distribution of previously reported CdSe nanoparticles.^[88] This model showed good agreement with a majority of the averaged properties of the synthesized nanoparticles, thus showing the efficacy of such models to describe nucleation and growth, and to facilitate a higher level of control over nanoparticle synthesis. Based on these single droplet oscillatory studies, Shen et al.^[92] then developed an oscillatory flow reactor for exchange reaction studies using inline absorption spectroscopy. This approach allowed for very low material consumption since reagents could be “recycled” through repeated flow reversal. Here, the evolution of the absorption features with time was observed, through the use of optical fibers on opposing sides of the tubing. Such an oscillatory flow reactor allows for fast mixing without additional mixing units, and precise characterization of certain reactions. However, it should be noted that the approach is inherently limited in terms of throughput. While absorption measurements in continuous-flow systems have been successfully executed,^[85] detection in segmented flow is somewhat limited due to scattering at the droplet-carrier fluid interfaces

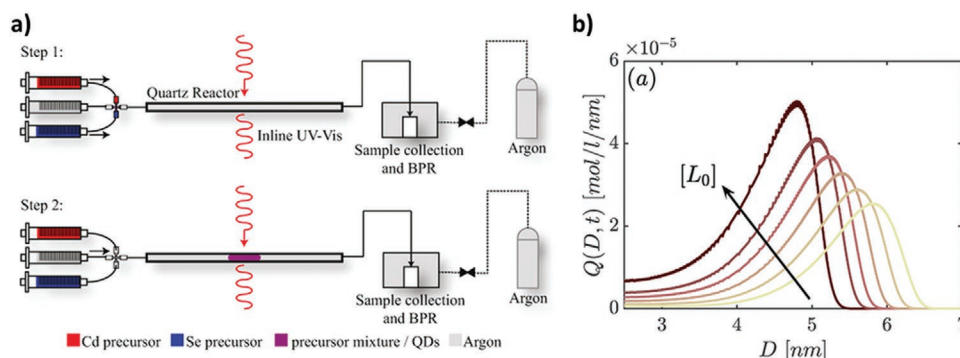


Figure 5. a) Schematic of a microfluidic platform with syringes for delivering precursors, a quartz reactor for absorption measurements, and collection unit. b) Dependence of the ligand concentration $[L_0]$ on the distribution of particles with the diameter D and time $t = 1200$ s. Adapted with permission.^[94] Copyright 2018, American Chemical Society.

and competing signals from the carrier fluid.^[93] The use of an inert gas (instead of an oil) is advantageous in this respect, as it removes the problem of absorbance by oils.^[93] For example, Lazzari et al.^[94] reported a method using a quartz reactor for inline absorption analysis in an argon atmosphere. Optical measurements were taken at 5 s intervals (with an integration time 40 ms) on stationary droplets (Figure 5a). This system was used to study the growth of CdSe nanocrystals in different ligand environments. Through stopped-flow operation, a study of an individual droplet over time was achieved, however with a loss in time resolution. In the course of this ligand study, a set of three ligand parameters were scanned; the ligand association rate constant, the ligand elimination rate constant, and the initial free ligand concentration. In all three cases, the size distribution of the nanoparticles at different time points was recorded and linked to the ligand parameter (Figure 5b), as well as the average number of ligands, monomer concentration, QD concentration, and bound ligand concentration as a function of time. The obtained parameters were fitted to an appropriate model to draw conclusions on the kinetics underlying ligand-mediated growth.

A sophisticated, multiparametric detection platform was recently presented by Baek et al.,^[35] and comprised six units connected in series with a mixing, aging, growth, shell formation and annealing elements, and a terminal PL/absorption

detection cell (Figure 6a). The first three units were used to grow InP cores, which were furnished with a ZnS shell in the two shell formation units, which themselves contain ten channels. The InP core particles were synthesized with diameters of 2 and < 5 nm with ZnS shells, with the resulting particles having a lowermost 42 nm full width at half maximum (FWHM) of the PL peak and a photoluminescence quantum efficiency (PLQE) of 40%. The small, monodisperse core-shell particles with relatively high quantum efficiencies are particularly impressive since they are heavy metal free. While the in situ emission measurements yielded sharp peaks (Figure 6c), the absorption features were less sharp, due to the lower signal-to-noise ratio of in situ absorption measurements compared to PL measurements. In general, obtaining superior absorption data is an important goal for nanoparticle systems, not only for concentration and production yield analysis, but also to gain more knowledge about the electronic states within nanoparticles.

The more analytics that can be integrated within a microfluidic platform, the richer the experimental data set and the deeper the resultant analysis. Beyond photoluminescence-based analytics, X-ray studies also provide a wealth of important information on nanoparticle character. Although there have been more X-ray studies on noble metal nanoparticles than QDs, there are still some notable reports in the literature. For example, Sun et al.^[59] studied the growth of CdSe QDs with

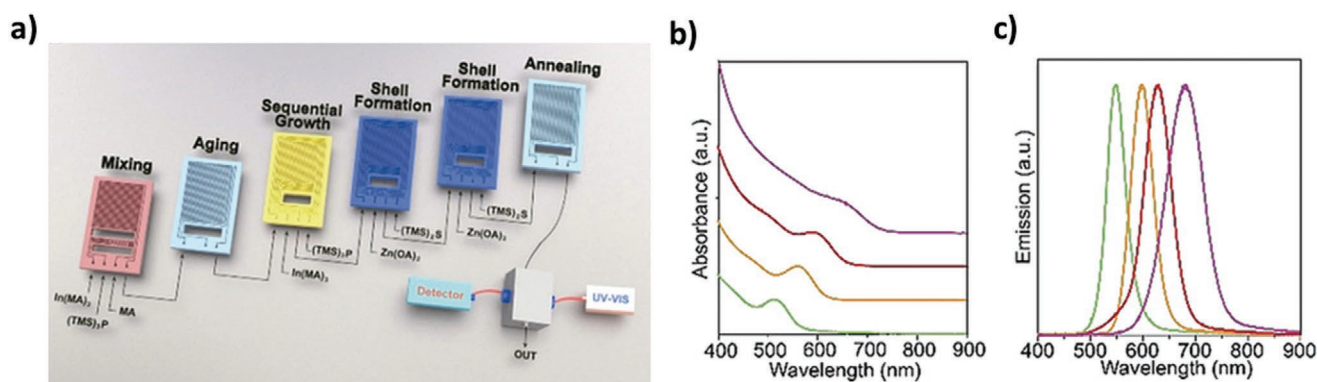


Figure 6. a) Multistage microfluidic platform for the synthesis of InP/ZnS nanoparticles and online characterization via absorption and PL detection. b) Absorption and c) PL spectra from online measurements. Reproduced with permission.^[35] Copyright 2018, Wiley-VCH.

inline EXAFS and online PL and absorption spectroscopy. By monitoring the consumption of selenium ions, the authors were able to follow the growth of CdSe nanocrystals and to propose a kinetic mechanism, demonstrating that rapid particle growth was complete within 3 s. In this work EXAFS could be used to study the whole reaction from 0 to 8.1 s. While useful, EXAFS studies are however limited to detecting the concentration of single ionic species, and cannot detect structural changes or yield information on optical properties. In a related study, Chan et al.^[56] revealed the use of XAS and stopped-flow absorption spectroscopy for ion exchange experiments on Ag₂Se and CdSe, demonstrating some problems associated with data extraction in flow. While in-flow operation could allow for XAS measurements and time-dependent structural studies, the low signal-to-noise ratios and small energy range could not allow for EXAFS analysis of the sample.

QDs are popular materials due to the wide range of potential applications in optoelectronic and biological fields. Automated, characterization-integrated QD synthesis platforms provide for the possibility to design bespoke materials according to the desired application, with potential for (understudied) scale-up for industrial production.^[95]

3.3. Metal Halide Perovskite Nanocrystals

Perovskite nanocrystals have received a tremendous amount of attention over the past five years owing to their outstanding promise in optoelectronics.^[96] Such materials exhibit intense PL over the entire visible spectrum and near infrared, size- and composition-tunable PL and excellent defect tolerance.^[97] Lead-halide perovskites (LHPs) have received the greatest attention, with the most common structure being ABX₃ (where A is the cation, B is Pb, and X: Cl, Br, I, with cesium (Cs), methylammonium (MA), and formamidinium (FA) the most commonly used A-site cations). The LHP crystal lattice has a strongly ionic character, which allows nanocrystals to form even at room temperature,^[98] and to undergo postsynthetic anion exchange much more readily than other QDs.^[98] Green- and red-emitting LHP nanocrystals show external quantum efficiencies (EQEs)

of 6–9%,^[96] while blue-emitting LHP nanocrystals have maximum reported EQE of 1.5%.^[99] However, it should be noted that LHP nanocrystals with pure color PL in the red are still difficult to obtain.^[97,100] A major problem with LHPs at the current time relates to their chemical and physical instability,^[97] arising from their low lattice formation energies. Their low temperature resistance, oxygen sensitivity, and high surface-to-volume ratio also make them highly unstable under atmospheric conditions and in aqueous environments. Although water stable LHP nanocrystals have been reported,^[101] a long term stability study has yet to be shown.^[98] The instability of LHP nanocrystals has drawn attention to their ligand chemistry^[68,102] and to possibilities for encapsulation.^[103] Due to concerns over the toxicity of lead, there have been efforts to identify lead-free alternatives. While good progress has been made, these currently lag some way behind LHP nanocrystals, with lower stabilities and efficiencies.^[77]

LHP nanocrystals are ideal candidates for study in microfluidic reactors, as nucleation, growth (<10 s), and ion-exchange are very fast, they do not require sequential growth of crystalline shells and their synthesis requires only moderate temperatures. The first demonstration of LHP nanocrystal synthesis in a tubing-based microfluidic reactor was by Lignos et al.,^[104] who synthesized stable red-emitting quaternary and quinary nanocrystals, while performing inline PL and absorption measurements. The study of Cs/FA–Pb–Br/I for the synthesis of red-emitting nanocrystals was obtained from a batch-synthesis protocol,^[105] and then subjected to parameter scanning to obtain optimized reaction conditions. Subsequently, these parameters were cycled back to the batch process. Here, the microfluidic platform was proposed as a parameter screening stage to realize ideal reaction conditions to form stable particles with PL between 700 and 800 nm (**Figure 7a**). Additionally, an automated script was used with preset parameters that are scanned and eventually analyzed in sum. A similar platform was subsequently used by the authors^[106] to study the nucleation and growth of blue-emitting formamidinium LHP nanocrystals using PL spectroscopy. The particles were characterized through their PL from 440 to 520 nm and tuned through changing ion composition by variation of the ratio

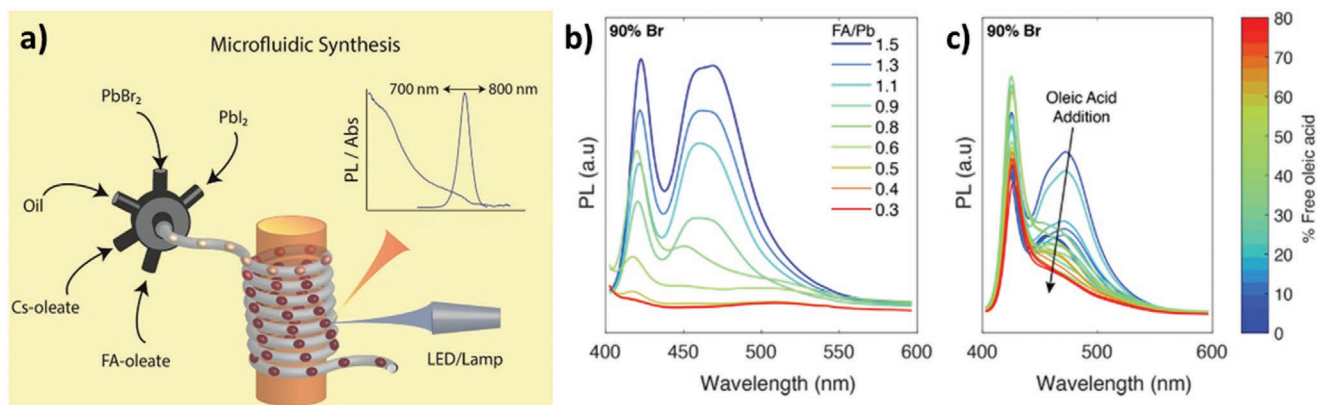


Figure 7. a) Schematic of the synthesis of LHPs in a microfluidic segmented flow reactor, with tubing conveying the reaction solution around a heating rod, with fiber optics for PL detection and a multiple inlet union junction for precursor mixing. Adapted with permission.^[104] Copyright 2018, American Chemical Society. b) PL spectra with the effect of the FA/Pb ratio at a set Br/Cl ratio, as well as c) the influence of the solvent access in the droplets. Reproduced with permission.^[106] Copyright 2018, American Chemical Society.

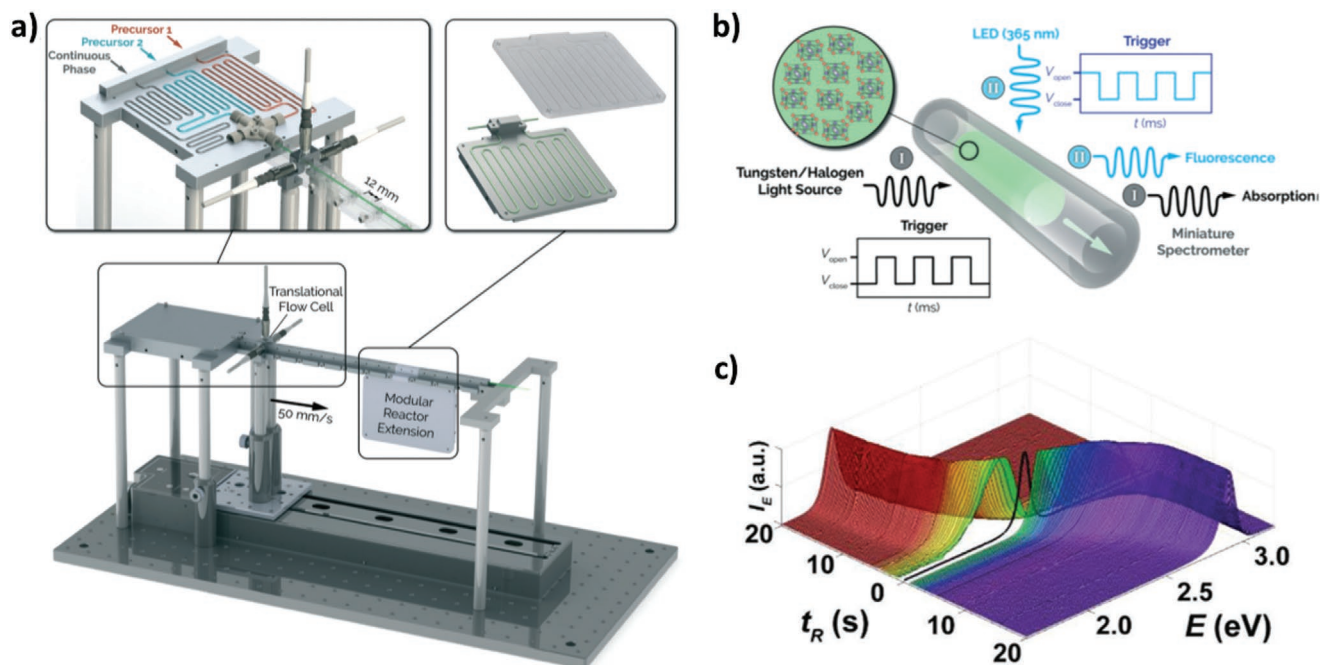


Figure 8. a) Schematic of a microfluidic platform with mixing units for every precursor (black, blue, and red) and droplet formation in a t-union with optical characterization using a movable optical fiber cell. b) Schematic of a droplet (green) in tubing (gray) showing the optical detection system with an absorption light source from the left (I) or LED from top (II) and a detector on the left (I, II). Adapted with permission.^[108] Copyright 2017, Royal Society of Chemistry. c) PL spectra of a halide exchange of CsPbBr₃ with ZnI₂ and ZnCl₂ mapping the intensity, time, and energy of PL. Adapted with permission.^[109] Copyright 2019, Wiley-VCH.

from FA-to-Pb and Br-to-Cl in multiple variations, as well as with the reaction temperature and the concentration of precursors and particles in solutions (Figure 7b). The setup allows for the study of multiple parameters associated with nanocrystal synthesis, thus providing a multidimensional parameter map. This kind of mapping of growth- and nucleation-related parameters would take an unacceptable amount of time and material using classical flask-based approaches. Indeed, for a reaction time of 7 s and stabilization time, every parameter set takes maximum 12 s^[106] with a droplet size of ≈0.07 μL (assuming a droplet diameter of 500 μm).^[106] When looking at 13 000 parameter sets (13 temperatures, 10 FA-to-Pb ratios, 5 Br-to-Cl ratios, 20 Cs percentages^[106]), the described microfluidic setup would take ≈2 days and use 0.004 mL of reagents. Assuming 10 syntheses per day, this encounter would on the other hand take many years and many liters of sample in a classical batch setup. Importantly, the authors highlight the use of parameter scanning for the determination of ideal reaction conditions, which can then be transferred back to the bulk. However, it is worth mentioning that this microfluidic platform can also be used to study reaction kinetics to understand the nucleation and growth of QDs, as well as a tool to synthesize QDs faster, more uniformly and with far less manual work.

A fully automated optofluidic platform that integrates fluorescence lifetime measurements in droplet-based flow for the real time extraction of lifetimes decays of CsPbX₃ nanocrystals was very recently reported by Lignos et al.^[107] Concurrent time-integrated PL and time-correlated single photon counting (TCSPC) measurements demonstrated the dependence of the fluorescence lifetime on the nanocrystal composition, reagent

ratio (Cs/Pb and Br/I) and temperature. This platform nicely illustrates the great potential of microfluidic platforms with their small reaction volumes (200 nL per measurement), fully automated operation and reduced screening times (≈1000 lifetime measurements in 5 h of operation) for the detailed mapping of parametric space.

A sophisticated modular microfluidic platform was also developed by Epps et al.^[108] as a tool for parameter screening and synthesis optimization of LHP nanocrystals. This platform includes precursor premixing for mass- and temperature uniformity, and a translational flow cell for optical characterization (in contrast to previous stationary optical units). The automated workflow (Figure 8a) consisted of initial precursor mixing on a heating platform and subsequent droplet formation in a cross-union piece. The reaction took place in tubing, which is optically accessible at fixed points along the flow cell. This setup allowed for simultaneous collection of PL and absorbance in every reaction droplet by rapidly alternating between a broadband light source (for absorption) and an LED light source (for PL), both feeding into a single spectrometer (Figure 8b). This approach allowed for the continuous acquisition of both types of spectra throughout the synthesis. The fiber optic mount extends along the flow cell (Figure 8a), allowing for sampling at different time points in the synthesis, yielding information on early reaction kinetics and the final nanocrystal characteristics. The authors highlighted multiparametric parameter scanning as a tool for growth characterization of LHP nanocrystals. Assuming a volume of 20 μL per spectra and a rate of 30 000 spectra per day, the approach significantly outperforms bulk methods and offline characterization. The same platform

was later elaborated into a new concept coined the “quantum dot exchanger” (QDEX),^[109] which allowed the kinetics of anion exchange reactions of LHP nanocrystals to be probed (Figure 8c). PL and absorption spectra were recorded for different reaction times and precursor ratios, allowing for fast parameter space mapping of the exchange reaction. The authors were able to identify a three-stage anion exchange process, suggesting that an initial pH disruption of the QD surface leads to removal of surface ligands, revealing unoccupied sites. Moreover, it was hypothesized that these vacancies are then replaced with halide ions, with a new ligand shell forming around the QD. The halide ions then move to the QD center, leaving vacancies that are filled by further halide ions or ligand molecules. The mechanism was relatively slow for iodide exchange due to the large size of the ions limiting their diffusion, a fact that concurs with known difficulties when working with iodide LHP nanocrystals. This work highlights the utility of automated microfluidic platforms in extracting previously unknown information regarding early time processes, and showcases the value of optical detection methods in studying nucleation, growth, and exchange reaction kinetics.

3.4. Conjugated Polymer Nanoparticles (CPNs)

The study of semiconductor nanoparticles has not been restricted to inorganic crystalline materials, with much recent interest in the synthesis and use of organic semiconductors. The π -conjugation along the backbones of conjugated polymers gives rise to energy bands akin to inorganic semiconductors, with high intra- and interchain mobility of charged species.^[13] Many of these polymers exhibit extremely high extinction coefficients, and large intrinsic PLQEs. Furthermore, they lack the intrinsic toxicity of heavy metals and thus are excellent base materials for making fluorescent nanoparticles. CPNs have been intensively studied and have demonstrated great success as biomedical imaging and therapeutic agents,^[5,48,110,111] and as components in organic LEDs and photovoltaics.^[13,112–114] The optical properties of CPNs are strongly correlated to the nature of the polymer, its side groups, chain length, and aggregation state. Functional groups on the side chains of the polymers, or on the capping agents, provide facile routes to the conjugation of further functional units.^[13,46,115] Although CPNs are sometimes less chemically and physically stable than their QD counterparts, and can exhibit interchain quenching,^[116] they are stable toward photobleaching and have a bright and stable PL with a reported photoluminescence quantum yield (PLQY) of up to 60%.^[48,117]

CPNs are most commonly synthesized by solvent exchange from a good solvent to an excess of a poor solvent. This poor solvent can be either miscible with the good solvent resulting in direct formation of solid nanoparticles (reprecipitation), or immiscible leading to formation of solid nanoparticles after removal of the good solvent (miniemulsion). Growth of the particles proceeds via coagulation and condensation of the polymer, which is stabilized by surfactants in solution.^[116,118] Collapse of the polymer chains into compact coiled structures allows close proximity and extensive inter- and intrachain interactions,^[13] with interchain energy transfer causing a red shift

in the PL spectrum. In small CPNs with a flexible backbone, collapse causes dominant intrachain interactions, which leads to a red shift in the absorption spectra due to the creation of new nonradiative deactivation pathways.^[119] However, when the polymer has a rigid backbone, coiling causes interruption to the π -conjugation yielding a shorter conjugation length, which leads to a blue shift of the absorption spectrum. An important aspect of synthetic work going forward will likely be hybrid CPN materials, incorporating QDs, noble metal nanoparticles, or upconversion nanoparticles (UCNPs).^[13]

The synthesis and characterization of CPNs in microfluidic platforms, especially with integrated optical detection, lag somewhat behind systems for QDs. Nevertheless, there are compelling reasons why the field has much promise for the future. Nanoprecipitation and miniemulsion in flask-based experiments tend to yield polydisperse nanoparticles due to poor mixing, whereas microfluidic reactors provide for much faster mixing. In microfluidic systems, control over size, population dispersity, uniformity, and tunability of the surface through antisolvent and solvent tuning is possible,^[120] and has been demonstrated for various other types of nanoparticles made by nanoprecipitation.^[33,46,121,122] For example, Kuehne and Weitz^[123] demonstrated the synthesis of monodisperse polyfluorene (PFO) nanoparticles (with sizes between 150 nm and 2 μ m) through the control of droplet size. The synthesis was conducted in a PDMS chip, with a Parylene-C coating being used to provide good solvent resistance. With particle polydispersity below 10%, this approach nicely illustrates the advantages that microfluidics brings to the synthesis of CPNs. Similarly, Abelha et al.^[124] demonstrated the generation of F8BT (poly(9,9-dioctylfluorene-*alt*-benzothiadiazole)) and cyano-substituted poly(*p*-phenylene vinylene) (CN-PPV) CPNs in a poly(ethylene glycol)–poly(lactide-*co*-glycolide) (PEG–PLGA) matrix. Significantly, the matrix did not affect the optical properties of the particles, but served as a neutral host that could be advantageous for many biomedical applications. The particles had high PLQYs (of up to 55%), with sizes between 140 and 260 nm, and polydispersities below 1%, with control over size achieved by modulating the ratio of organic solvent to aqueous phase. The antisolvent used in CPN synthesis is typically water, which is advantageous for biomedical applications, although there has been some work on supercritical fluids for solvent free NPs. For example, Couto et al.^[122] showed the synthesis of poly(3-hexylthiophene) (P3HT) CPNs via a supercritical antisolvent process rendering solvent-free particles. The use of supercritical CO₂ in this regard also allows for the variation of pressure, viscosity, and density of the antisolvent.

Although the above studies nicely demonstrated the advantages of microfluidics in synthesizing high quality CPN products, they did not leverage any integrated analytics or real-time characterization. However, there has been the occasional demonstration of such facility. For example, Schütze et al.^[125] showed the reprecipitation synthesis of CPNs using a block copolymer poly(fluorine ethynylene)-*block*-poly(ethylene glycol) (PFE-PEG) in a glass device (Figure 9a). The kinetics of particle formation was probed by placing the chip in a microscope for PL measurements. Through measurement of the fluorescence of a dye incorporated in the polymer solution, the authors concluded that mixing was the limiting step for NP formation.

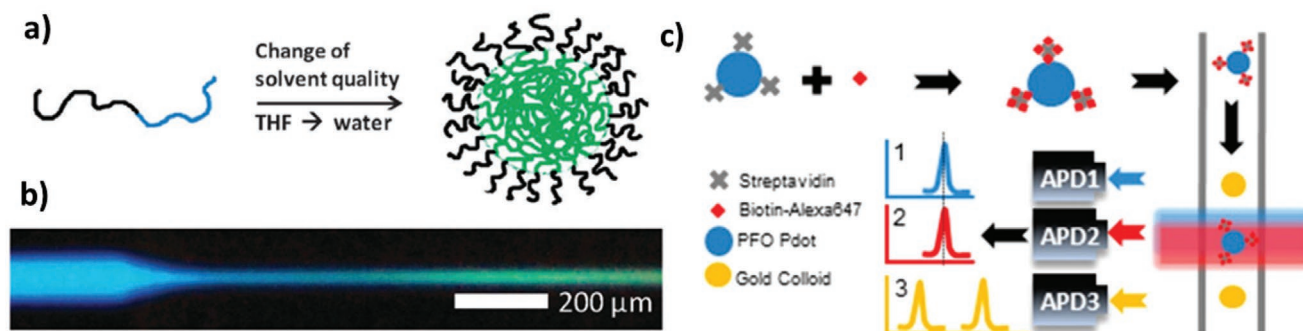


Figure 9. a) Schematic of block copolymer nanoparticle reprecipitation, with b) fluorescence imaging of the continuous synthesis of PFE-*block*-PEG CPNs with a shift from blue to green fluorescence. Adapted with permission.^[125] Copyright 2011, Royal Society of Chemistry. c) Schematic of PFO Pdot functionalization with biotin and streptavidin for single particle detection in a confocal microscope setup. Adapted with permission.^[126] Copyright 2018, American Chemical Society.

Such a PL detection technique allows for a broad view of the entire flow, which affords a comprehensive overview of reaction kinetics (Figure 9b). In contrast, Jung et al.^[126] demonstrated a flow platform incorporating inline, confocal PL detection. Although CPNs were not synthesized in the setup, they were characterized inline. Specifically, the number of biomolecules on the CPNs was studied, allowing direct quantification of the average number of biomolecules per particle. A schematic of the platform used for CPN functionalization and subsequent analysis with PL in flow is shown in Figure 9c. This setup provides for low detection limits, and although not used for automated synthesis and characterization, it highlights the potential of microfluidic platforms for the handling of CPNs and single molecule studies. Accordingly, it can be seen that use of PL and absorption detection for the quantitative analysis of nanoparticles in flow enables single-particle resolution.

3.5. Carbon Dots

The growing interest in nontoxic nanomaterials with bright PL has focused on a few useful materials with desirable properties. Among these are CDs. CDs are sub-10 nm spherical particles consisting of layered graphene sheets, possessing bright PL with broadly tunable emission, high photostability, and low

toxicity.^[7] CDs have π -conjugated domains in their core, and exhibit room temperature phosphorescence, which has raised much interest in the scientific community, particularly for use in white-light-emitting diodes (WLEDs), bioimaging and biosensing, and for photothermal and photodynamic therapy.^[6] While promising, CDs remain under investigated, and are currently limited by an inability to precisely tune emission wavelengths, high levels of self-quenching, and low brightness at longer wavelengths. Accordingly, more fundamental research into this class of material is needed.^[127]

CDs have been studied using microfluidic systems with PL and absorption spectroscopy.^[128] CD PL is dependent on several factors, including dopant and ligand concentrations and surface morphology, but not size or composition. This makes the synthesis of CDs with target properties more challenging than for QDs.^[128] A three-step procedure of selecting precursors, solvents, and additives, finding reasonable combinations and then summarizing data was performed manually in this study by Lu et al.,^[128] but resembles the workflow of algorithm driven data analysis, suggesting the potential of such platforms for automated operation. In addition, Berenguel-Alonso et al.^[38] presented a solvent-resistant ceramic microreactor with inline PL and absorption detection^[129] for the synthesis of CDs. The reactor consisted of a circular, low temperature cofired ceramic (LTCC) flow unit with a window for PL imaging (Figure 10a,b).

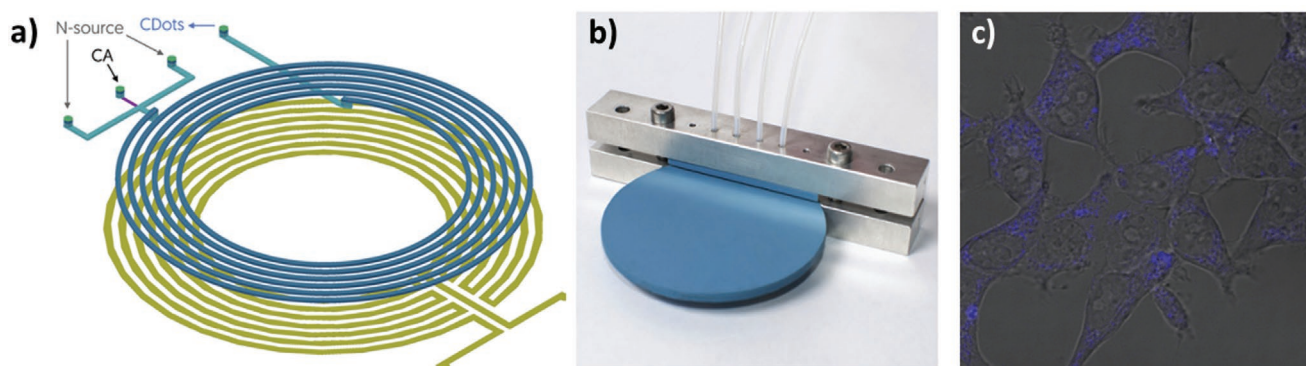


Figure 10. a) 3D schematic of the LTCC microreactor with inlets and outlet (blue) and heating unit (yellow). b) Picture of the reactor with metal tubing fixation. c) Combined image of HEK293 cells and PL image of CD loaded cells. Adapted with permission.^[38] Copyright 2019, Elsevier.

The reactor allowed for the systematic study of temperature, pressure (up to 17 bar) and precursor chemistry, and suggested ideal conditions for the production of highly photoluminescent CDs at 17 bar and 190 °C. Importantly, the ceramic reactor allows for the study of harsh conditions inaccessible to conventional microfluidic reactors. Finally, the work also included studies of the CDs with HEK293 cells using brightfield and fluorescence imaging (Figure 10c), and toxicity testing. CDs owe their popularity to their biocompatibility and low toxicity; therefore it is of vital importance to evaluate their degradation to ensure that the by-products are also nontoxic. Such a question is well-suited for future investigation using high-throughput parametric screening using microfluidic platforms.

3.6. Noble Metal Nanoparticles

Nanoparticles of noble metals and their alloys can exhibit localized surface plasmon resonance (LSPR) due to resonant oscillations of the electric field of incident light and free electrons in the metal. This electron oscillation frequency is strongly correlated to particle composition, size, and shape.^[130] Their strong absorption, low toxicity, high electron density, and facile surface functionalization make noble metal nanoparticles highly useful in a range of biological systems. They allow for functional group attachment to their surfaces through covalent (dative) and noncovalent binding, with a notable affinity between gold and thiols.^[131] Noble metal nanoparticles do not typically exhibit PL, however particles of a certain size (which varies from metal to metal, and is in the range of $\approx 1\text{--}3$ nm for gold^[132]) do exhibit PL. These particles, termed nanoclusters,^[133] see the continuous bands of the bulk metal split as the structure is reduced in size, forming discrete energy levels through

which electrons can be excited, leading to photon emission upon relaxation.^[7] Although many of these nanoclusters have only modest or low PLQY, there are some specific cluster sizes that exhibit brighter PL that can be further enhanced by electron-rich ligands or a core-shell structure involving different metal-ligand compositions.^[1,132]

Microfluidic studies on noble metal nanoparticles have primarily focused on the use of X-ray and absorption spectroscopy to analyze growth and nucleation, yielding detailed information about structure and electronic state composition. For example, a microfluidic study on Au-Ag core/shell nanoparticles was performed by Knauer et al.^[134] using online absorption spectroscopy. This system was fully automated with programmed parameters for flow rate variation during synthesis (Figure 11). Both the particle size and shell thickness could be precisely controlled by variation of the flow rates of input streams. Furthermore, offline characterization was performed by differential centrifugal sedimentation (DCS), transmission electron microscopy (TEM) and X-ray photoelectron spectroscopy (XPS). In another study, Karim et al.^[60] reported a SAXS and X-ray absorption fine structure (XAFS) study of 1 nm Pd nanoparticles. XAS measurements allowed for the detection of the coordination number of Pd (EXAFS) and the percentage of Pd in solution (XANES), yielding information on the amount of Pd-Pd, Pd-O, Pd-C, and Pd acetate in the reaction solution. Analysis of the SAXS data also shed light on the diameter and number of particles, indicating a two-step growth process with an initial fast and a secondary slower step.

While SAXS measurements are valuable in the analysis of structural changes, XAS is useful for determining the electronic state of a system. Tofighi et al.^[57] studied the growth of Au nanoparticles in a microreactor at early reaction times. Based on this work, Tofighi et al.^[58] later demonstrated the

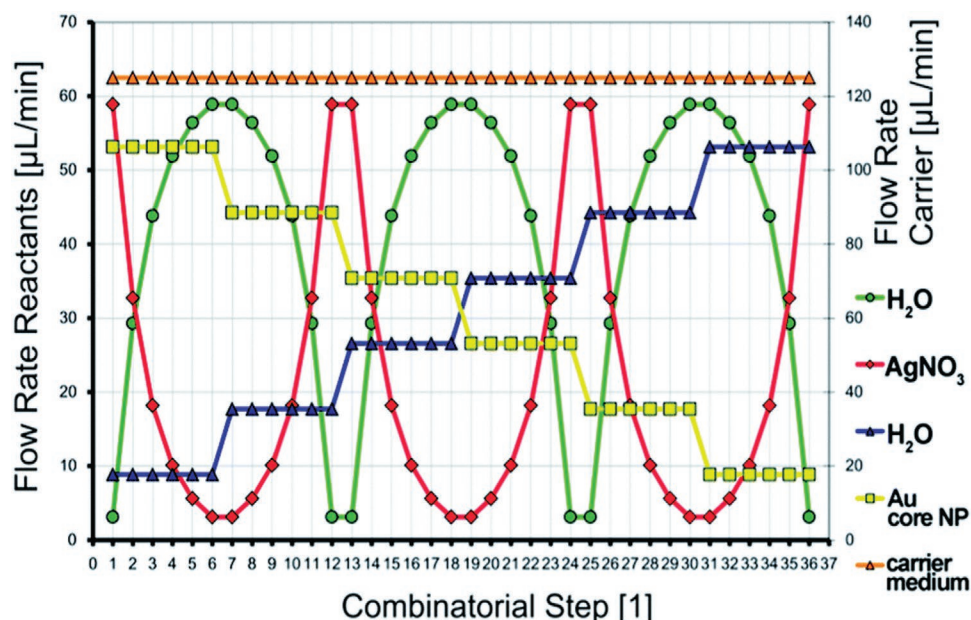


Figure 11. Preset parameter conditions for the automated synthesis of Au-Ag core/shell nanoparticles, with descending Au core flow rate (yellow), ascending water flow rate (blue), and counteracting oscillatory AgNO_3 (red) and water flow rates (green) at a stable carrier medium flow rate (orange). Reproduced under the terms of the CC-BY 3.0 license.^[134] Copyright 2014, The Royal Society of Chemistry.

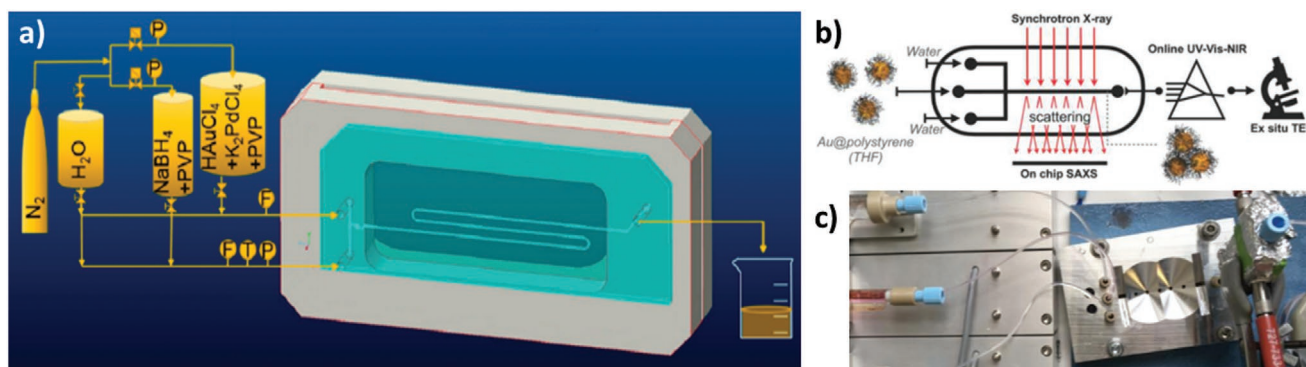


Figure 12. a) Schematic of a microfluidic chip with an X-ray transparent window made of Si-glass with a stainless steel frame for support. Reproduced with permission.^[58] Copyright 2019, American Chemical Society. b) Schematic of a Kapton chip in a stainless steel frame for SAXS measurements; Adapted with permission.^[135] Copyright 2019, American Chemical Society, with c) an image of the UV-vis flow cell; Adapted with permission.^[202] Copyright 2019, American Chemical Society.

combination of XAS, Fourier-transform infrared spectroscopy (FTIR), and XPS to probe the catalytic activity of AuPd nanoparticles in the oxidation of CO. FTIR was used to determine the active surface sites of the metal nanoparticles, where Au particles have a neutral and Pd a positively charged surface, and Au-Pd alloys have neutral Au and Pd surface sites. An ideal Au:Pd ratio of 3:7 was determined for the oxidation of CO.

Thiele et al.^[130] presented a microfluidic reactor with multiple stages for Au seed formation and a residential channel for particle growth. The two units were not directly connected, which limited automation potential, and necessitated manual collection and reinjection of samples. Specifically, growth was followed by absorption spectroscopy through an optical detection window near the outlet, with peak positions being correlated to the size of the Au particles. Moreover, parametric screening was executed by varying the concentration and compositions of the counter ions, and then studying their effect on particle shape.

The union of absorption and X-ray studies was most recently reported by Merckens et al.^[135] in a 3D flow-focusing device (Figure 12a) for the study of the solvent-induced self-assembly of Au nanoparticles with SAXS and absorption measurements (Figure 12b). This system provided for a time-resolution of 4.8 ms, and a maximum residence time of 2.8 s, which was limited by the beam size and flow speed on the early time scales, and by the channel length and flow speed for longer times. Pre-formed Au nanoparticles were induced to form clusters when their polystyrene shells experience a hydrophobic collapse upon solvent-exchange. While not being a multiparametric study, this work combines absorption and SAXS measurements with numerical simulations for advanced data interpretation, and thus shows a complementary use of two distinct detection techniques and theoretical studies.

X-ray detection techniques are powerful tools for uncovering the structural and electronic state of nanoparticles, but they are either limited to long integration times or typically involve a reserved time slot for experiments at a synchrotron facility. While access to such facilities has improved in recent years,^[136] experiments still require application months in advance, around the clock work for a few days and then months of data analysis and interpretation. Such effort makes these methods

laborious and less widely applicable, but if used wisely can yield vital and otherwise inaccessible data.

3.7. Rare-Earth Upconversion Nanoparticles

UCNPs doped with rare-earth elements, typically Er and Yb, are most popular in biological applications, where highly penetrating red/infrared light can be used to excite nanoparticles in situ, with upconverted emitted light being used to trigger, for example, targeted bond breaking or drug release.^[137] Further advantageous properties of UCNPs include their high stability and long radiative lifetimes. Upconverting PL stems from multiphoton absorption, energy transfer, and emission of high energy photons.^[138] UCNPs are sensitive to concentration quenching, where PL is reduced at high dopant concentrations due to interparticle energy transfer. This imposes constraints on dopant concentrations and size of the particles, and limits practically achievable brightnesses.^[8] The microfluidic synthesis of UCNPs was demonstrated by Liu et al.^[139] using a tubular microreactor, with reaction times below 10 min and temperatures of 255 °C. The studied UCNPs were cubic α -NaYF₄:Yb,Er particles, which subsequently formed the hexagonal phase exhibiting upconverting activity through Ostwald-ripening. While the flask-based synthesis of the hexagonal form takes multiple hours at elevated temperatures (300 °C),^[140] use of a microfluidic environment enabled facile separation of the cubic and hexagonal phase formation, thus allowing for initial synthesis of the cubic phase in 10 min and at lower temperatures.^[139] It is clear that the study of UCNPs using microfluidic systems could be especially useful in understanding the effects of doping concentration, but so far this aspect is unexplored.

4. Advanced Automation and Analysis

As microfluidic platforms grow in power and complexity, the manual control and subsequent analysis of the resulting data sets becomes prohibitive. Accordingly, such complexity developments dictate the use of automated and “intelligent” control and analysis systems. The first automated, multidimensional

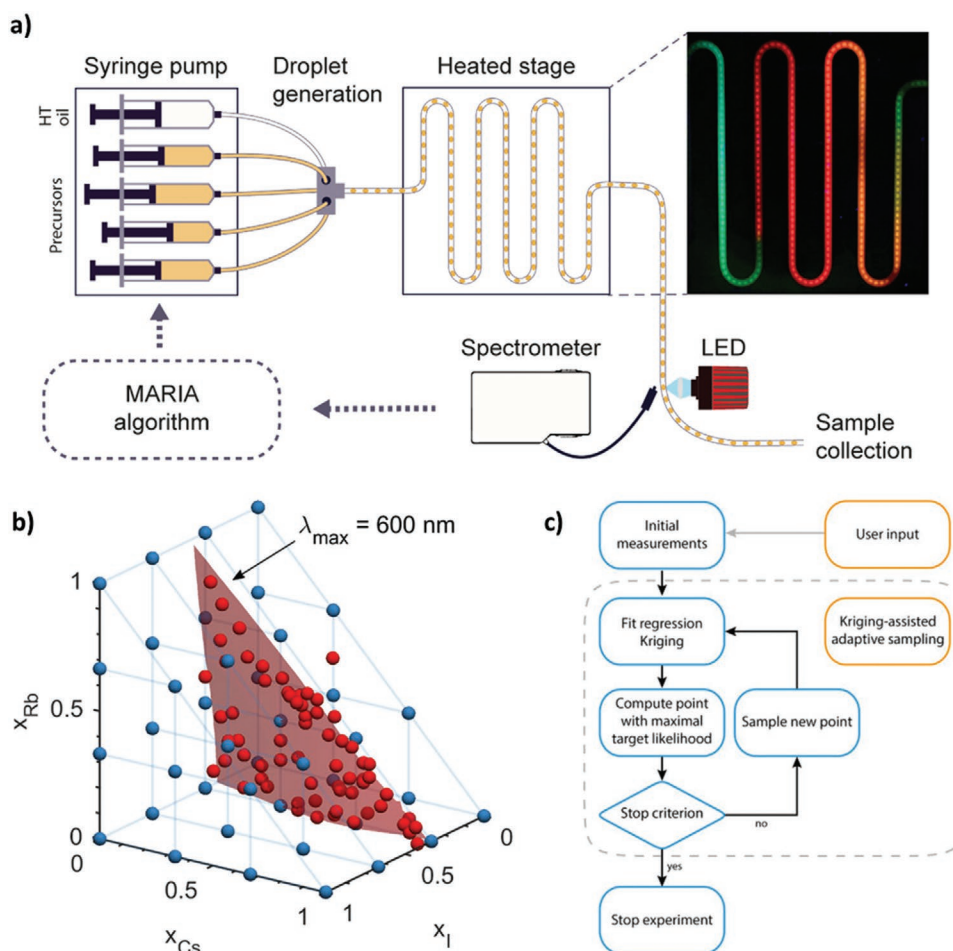


Figure 13. a) Schematic of an algorithm-controlled microfluidic platform with variable flow rates and online PL spectroscopy. b) A 3D parameter screen of Cs and Rb doping and halide ratio with the preset parameter (blue) and the parameters computed by the algorithm (red). c) The kriging algorithm used for optimization of reaction parameters to achieve a preset goal. Adapted with permission.^[142] Copyright 2018, American Chemical Society.

parameter optimization in the synthesis of nanoparticles in microfluidics was reported by Krishnadasan et al. in 2007.^[63] In this study, the authors leveraged a stable noisy optimization by branch and fit (SNOBFIT) algorithm^[141] to scan the parameter space and a “dissatisfaction coefficient” to assess the success of individual experiments. Specifically, the approach was applied to the synthesis of bespoke CdSe QDs, where size, polydispersity, and PLQY could be controlled by variations volumetric flow rates and temperature. This work elegantly demonstrated the potential of integrating an algorithm for a target-oriented approach to synthesizing nanoparticles in microfluidics. More recently, the same group presented a fully automated microfluidic segmented-flow platform for the synthesis of hybrid organic–inorganic quinary (Cs/FA)Pb(I/Br)₃ and senary (Rb/Cs/FA)Pb(I/Br)₃ LHP nanocrystals (Figure 13a).^[142] Here, the automated system performs targeted multidimensional parameter scanning, with a control algorithm reading data from inline PL detection and using it to refine reaction parameters toward a target PL wavelength. This is achieved by employing a custom kriging algorithm, termed “multiparametric automated regression kriging interpolation and adaptive sampling” or MARIA. The kriging algorithm employs distance weighing interpolation, which has reduced “training”

requirements when compared to neural networks.^[143] Figure 13b illustrates the case of a 3D parameter scan, varying Cs doping (x_{Cs}), Rb doping (x_{Rb}), and halide ratio (x_I), toward a targeted emission of 600 nm for (Rb/Cs/FA)Pb(Br/I)₃. The algorithm takes in an initial set of user-defined parameter sets spanning a parametric space (blue dots in Figure 13b), and after executing the experiments and analyzing the results, fits a model that provides a “best guess” of parameters that will yield the target PL. After trying this best guess set, the algorithm refines the model and tries again, repeating for a fixed number of cycles, with the ultimate result being a list of distinct parameters sets that yield nanocrystals with the target PL (red dots in Figure 13b). Such a capability distinguishes MARIA from earlier kriging-based optimizations, which only returned a single value.^[143] Additionally, from the collected list of possible parameters, it is possible to analyze the data for further optimization, looking to minimize the emission FWHM or maximize fluorescence intensities, for example. Importantly, this system runs with minimal user input, requiring just the preparation of the precursors, filling of the syringes and definition of the initial parameter set. Such a target-oriented approach is extremely useful if desired properties are in demand. If, however, a general understanding

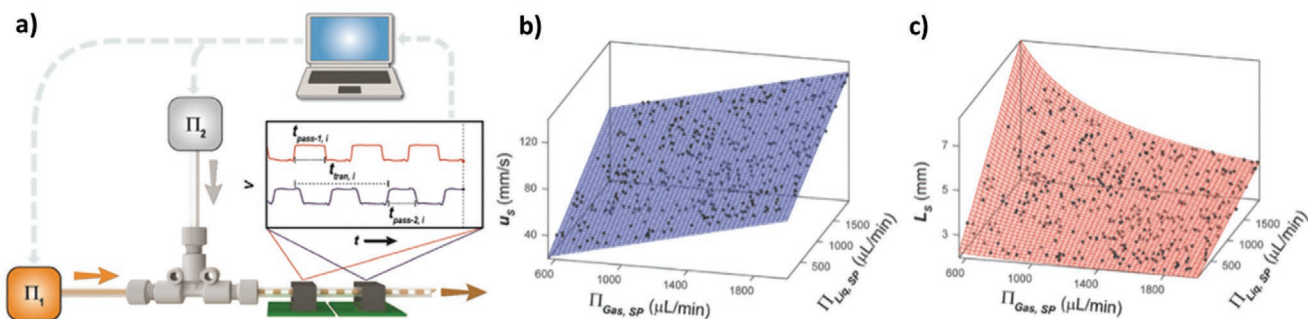


Figure 14. a) Schematic of the OVAL system with feedback from a control unit, and parameter scans of b) velocity and c) slug length with gas and liquid flow rates. Adapted with permission.^[144] Copyright 2019, Royal Society of Chemistry.

of nanoparticle nucleation and growth under different conditions is sought, or a broader understanding of the relationship between the reaction variables is required, then systematic scanning of a larger parameter space will suffice.

As described previously, Epps et al.^[108] developed an automated optical flow cell platform, integrating PL and absorption detection. In an extension of this work, the authors proposed an optical velocity and length sensor (OVAL), incorporating an integrated slug-counting algorithm (Figure 14).^[144] This system was used to conduct parameter space mapping of gas and liquid flow rates of the two-phase flow system. The OVAL sensor, in combination with a two-input, two-output fuzzy logic system (TITO FLS) algorithm was subsequently used to study the effect of mixing and slug velocity on LHP optical properties, indicating blue-shifted and broadened emission at higher slug velocities.

Artificial neural networks (ANNs) are machine learning algorithms that mimic a biological neural network, and thus represent a category of artificial intelligence (AI) algorithms.^[145] The use of ANNs in photonic nanoparticle synthesis should have interesting capabilities compared to previously used algorithms, however the development and implementation of ANNs is much more time consuming and by definition less intuitive. Nevertheless, ANNs show significant promise, and have already been used to good effect. For example, Orimoto et al.^[146] and Watanabe et al.^[147] used ANNs for the analysis of data originating from combinatorial CdSe nanoparticle synthesis.^[34] Briefly, the ANN proceeds through three steps for optimization. First, a synthesis with a set of predefined starting parameters is initiated. Next, the ANN obtains the output (properties of the nanoparticles) correlated to the input (parameter set) and computes an input–output trend. Finally, the input is changed to achieve an optimized output (in terms of CdSe nanocrystal properties), which involves generating new conditions, interpolating from the input–output data set and a sensitivity analysis. For each condition and property, a 2D landscape is used to show the property trend with changing conditions. Such an analysis yields a multidimensional data landscape showing the dependency of nanoparticle properties with every parameter. Such an approach is both accurate and sensitive, however it demands extensive training for the NN and the formation of an ensemble neural network (ENN) comprised of a number of component neural networks (CNNs). Indeed, while a well-trained ANN can predict outputs, even to values they were not trained with, training is very extensive. That said,

the use of ANNs seems very promising for the combinatorial synthesis of a range of nanoparticles.^[146]

A summary of the most relevant studies discussed in this review is provided in Table 1.

5. Outlook

Methods for the synthesis of photonic nanoparticles within microfluidic platforms have made excellent progress in recent years, confirming their utility in exploring complex reaction parameter spaces with concomitant savings in both reagent and time. However, there is still much potential to be unlocked, with the vision of automated microfluidic reactors as an indispensable tool in the discovery, optimization, and realization of photonic nanoparticles yet to be fully realized. Areas of potential include expanding the dimensionality of accessible parameter space (including temperature, time, pressure, a multitude of precursors, ligands, and solvents), further reducing material requirements through minimizing reaction volumes and increasing the rate and quality of information generation. Additionally, an area of special interest is the development of methods for effective nanoparticle sizing that work in flow and can be integrated into an automated microfluidic platform. In the following sections, we highlight some specific areas of potential and how innovation is likely to contribute to developments in the field.

5.1. Addressing Nanoparticle Toxicity

The use of toxic elements in photonic nanoparticles can only be justified if the benefits outweigh the potential harm. We are quite familiar with such a risk–benefit analysis in medicine, where for example the toxic side effects of chemotherapy drugs are tolerated due to the chance of successful treatment. In consumer electronics, small amounts of toxic metals are concealed inside the device, with leakage being highly unlikely. However, although toxicity at the point of use can be either eliminated or tolerated, the destination of these materials after use and/or disposal is extremely difficult to predict and contain. Consequently, it is preferable, wherever possible, to move toward materials with either no or minimal amounts of toxic elements within. This concept has had its impact already, for example

Table 1. Summary of relevant demonstrations of the nanoparticle synthesis optimization by microfluidics.

Material class	Material	Reactor type (material) ^{a)}	Type of flow	Heating method and range	Optical characterization	Main advantage	Refs.
Inorganic semiconductor nanoparticles	CdSe	Chip-based (glass)	Continuous flow	Hotplate (220–270 °C)	Online PL detection	Control over particle size through variation of temperature and flowrates	Krishnadasan et al. ^[80]
	CdSe	Chip-based (glass)	Continuous flow	Hotplate (160–255 °C)	Inline PL detection	Operated by a control algorithm for autonomous intelligent synthesis	Krishnadasan et al. ^[83]
	CdTe	Chip-based (PDMS/glass)	Segmented flow	ITO film-based heater (80–92 °C)	Inline PL detection	Picoliter droplets, integrated heating	Yao et al. ^[81]
	CdS-Cys	Chip-based (silica/glass)	Continuous flow	–	PL imaging	Spatial resolution	Sounart et al. ^[82]
	PBS	FlowSyn Multi-X system (Uniqsis Ltd., Cambridge UK (PTFE or stainless steel or Hastelloy C-276))	Continuous flow	Coil heater module (75–120 °C)	Online PL detection	Dual-temperature-stage reactor, automated operation with sample collection	Pan et al. ^[83]
	CdS-Cys	Chip-based (PDMS)	Continuous flow	–	Inline PL detection and absorption spectroscopy	Early time (1–100 ms) nucleation and growth kinetics	Seibt et al. ^[84]
	CdSe	Capillary-based (silica)	Continuous flow	Oil bath (195–300 °C)	Online absorption spectroscopy	Several microreactors	Toyota et al. ^[34]
	Cd ₂ Hg _{1-x} Te	Capillary-based (tube/quartz)	Continuous flow	–	Online PL detection and absorption spectroscopy	Reaction kinetics from seconds to hours, extraction of radiative and nonradiative decay	Kershaw et al. ^[85]
	CdSe and InP	Tubing-based (FEP)	Segmented flow	Cartridge heaters (160–220 °C)	Inline PL detection and absorption spectroscopy	Automated operation, oscillatory flow (single droplet tracking)	Abolhasani et al. ^[88]
	CdSe	Tubing-based (FEP)	Segmented flow	Cartridge heaters (240–300 °C)	Inline absorption spectroscopy	Oscillatory flow, biphasic system	Shen et al. ^[92]
Metal halide perovskite nanocrystals	CdSe	Capillary-based (quartz)	Segmented flow	Cartridge heaters (20–220 °C)	Online absorption spectroscopy	Combination with deterministic model, property prediction	Lazzari et al. ^[94]
	InP/ZnS, InP/ZnSe, InP/CdS, InAs/InP	Chip-based (silicon-Pyrex)	Continuous flow	Heating block (120–320 °C)	Online absorption spectroscopy	Multiple stages, high pressure and high temperature	Baek et al. ^[35]
	CdSe	Tubing-based (Kapton)	Continuous flow	(138–241 °C)	Inline EXAFS and online absorption spectroscopy	Combination of EXAFS with absorption spectroscopy	Sun et al. ^[59]
	CdSe to Ag ₂ Se	Chip-based (SU8-glass)	Continuous flow	–	Inline XAS, stopped flow online absorption spectroscopy	Combination of XAS and absorption spectroscopy, millisecond time resolution	Chan et al. ^[56]
	CdSe	Capillary-based	Continuous flow	Solder bath (225–300 °C)	Online PL detection and absorption spectroscopy	NN data processing of the large number of experimental sets (3387) suitable for analyzing large, complicated data sets (for new materials)	Watanabe et al. ^[147] Orimoto et al. ^[146]
	Cs ₂ FA _{1-x} Pb(Br _{1-y} I _y) ₃	Tubing-based (PTFE)	Segmented flow	Copper heating rod (25–130 °C)	Inline PL detection and absorption spectroscopy	Same point PL and absorption measurements during heating, automated screening	Lignos et al. ^[104]
	FAPbX ₃ , X = Cl, Br, I	Tubing-based (PTFE)	Segmented flow	Copper heating rod (25–150 °C)	Online PL detection	Automated operation, NC and NPL formation	Lignos et al. ^[106]
	CsPbX ₃ , X = Cl, Br, I	Tubing-based with flow cell (PTFE with PDMS)	Segmented flow	Copper heating rod (150–200 °C)	Online confocal PL detection and PL lifetime	Automated operation, combination of PL and PL lifetime, single-droplet measurements	Lignos et al. ^[107]

Table 1. Continued.

Material class	Material	Reactor type (material) ^{a)}	Type of flow	Heating method and range	Optical characterization	Main advantage	Refs.
Conjugated polymer nanoparticles	CsPbX ₃ X = Cl, Br, I	Tubing-based (FEP)	Segmented flow	–	Inline PL detection and absorption spectroscopy	Translational flow cell	Epps et al., ^[108] Abdel-Latif et al. ^[109]
	(Cs/FA)Pb(I/Br) ₃ , (Rb/Cs/FA)Pb(I/Br) ₃	Tubing-based (PTFE)	Segmented flow	Ceramic heating plate (180 °C)	Inline PL detection	Operated by a control algorithm (MARIA) for a target-oriented optimization	Bezinge et al. ^[142]
	CsPbBr ₃	Tubing-based (FEP)	Segmented flow	–	Inline PL detection	Operated by control algorithm (OVAL) for parametric study of slug velocity and length	Kerr et al. ^[144]
	PFO	Chip-based (PDMS/glass)	Segmented flow	–	Offline PL detection and absorption spectroscopy	Monodisperse particles, control over size	Kuehne and Weitz ^[123]
Carbon dots	F8BT and CN-PPV	Capillary-based (silica)	Continuous flow	–	Offline PL detection and absorption spectroscopy	PEG–PLGA matrix for biomedical applications	Abelha et al. ^[124]
	P3HT	Capillary-based (silica) in silicon/Pyrex microreactor	Continuous spray flow	(40–50 °C)	–	Supercritical antisolvent synthesis for solvent-free particles	Couto et al. ^[112]
	PFE-PEG	Chip-based (glass)	Continuous flow	–	Spatially resolved PL spectroscopy	Spatially resolved PL detection, mixing faster than particle formation	Schütze et al. ^[125]
	PDFD/PFO	Chip-based (PDMS)	Continuous flow	–	Inline confocal PL detection	Single particle detection	Jung et al. ^[126]
	–	Tubing-based (PTFE)	Continuous flow	Oil bath (180 °C)	Offline PL detection	Rapid screening over a wide parameter space	Lu et al. ^[128]
	–	Chip-based (LTCC)	Continuous flow	Screen-printed heating element (100–200 °C)	PL imaging	High pressure and temperature reactor	Berenguel-Alonso et al. ^[138]
	Au	Chip-based (PDMS/glass or silicon)	Segmented flow	–	Online absorption spectroscopy	Oscillatory flow reactor	Abolhasani et al. ^[67]
	Au	Tubing-based (PTFE)	Segmented flow	Resistive heating element (80 °C)	Online absorption spectroscopy	Automated operation, precise control over shell thickness	Knauer et al. ^[134]
	Pd	Chip-based (silicon/Pyrex)	Continuous flow	Pt heat exchanger (30–100 °C)	Inline SAXS and XAFS	Coolant and heater, small nanoparticles (1 nm), combination of SAXS and XAFS	Karim et al. ^[60]
	AuPd	Chip-based (silicon/glass/stainless steel)	Continuous flow	–	Online XANES	Small particles (1 nm), high catalytic activity	Tofighi et al. ^[58]
Rare-earth upconversion nanoparticles	Au	Chip-based (silicon/glass)	Continuous flow	–	Inline XAS	Small particles (1 nm), early reaction stage investigation (6 ms)	Tofighi et al. ^[57]
	Au	Chip-based (glass)	Continuous flow	–	Offline absorption spectroscopy	Dean-flow-micromixer	Thiele et al. ^[130]
	Au	Chip-based (Kapton)	Continuous flow	–	Online absorption spectroscopy and inline SAXS	Combination of absorption spectroscopy and SAXS, time resolution of 4.8 ms	Merkens et al. ^[135]
	α -NaYF ₄ :Yb,Er	Tubing-based (quartz)	Continuous flow	Oil bath (25–255 °C)	–	Short reaction time (<10 min), inline mixing	Liu et al. ^[139]

^{a)}EXAFS: extended X-ray absorption fine structure; FEP: fluorinated ethylene propylene; ITO: indium tin oxide; MARIA: multiparametric automated regression kriging interpolation and adaptive sampling; NC: nanocrystal; NN: neural network; NPL: nanoplatelet; OVAL: optical velocity and length sensor; PL: photoluminescence; PDMS: poly(dimethylsiloxane); PTFE: polytetrafluoroethylene; SU-8: SU-8 negative photoresist; XAFS: X-ray absorption fine structure; XANES: X-ray absorption near-edge structure; XAS: X-ray absorption spectroscopy.

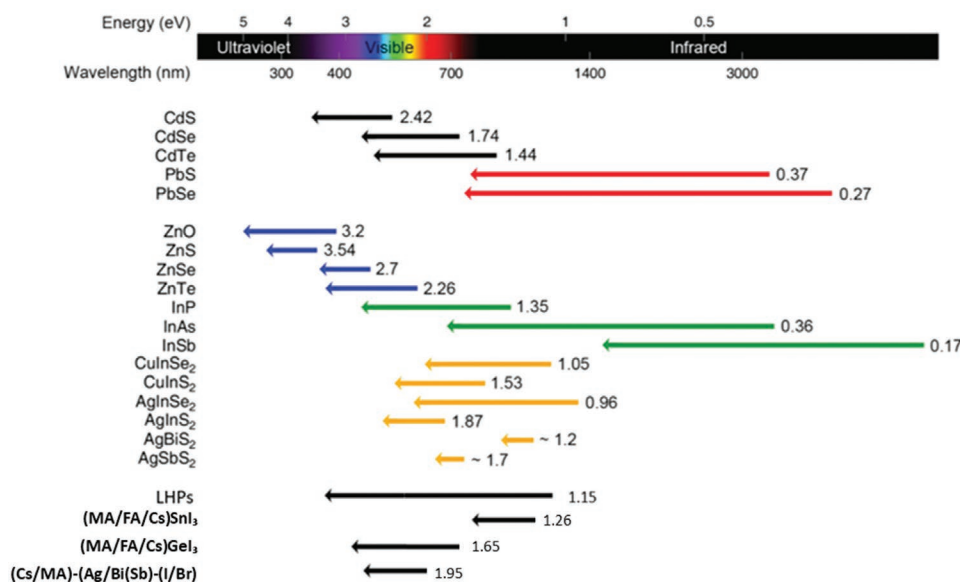


Figure 15. The bandgap ranges obtainable by size tuning of QDs,^[74] LHPs,^[203] and lead-free perovskites.^[133] Adapted under the terms of the CC-BY 4.0 license.^[74] Copyright 2019, Informa UK Limited trading as Taylor & Francis Group, The Korean Information Display Society.

inspiring Samsung to switch their QLEDs to InP for “cadmium free” displays and televisions.^[148]

The drive to improve heavy metal free nanoparticles is bearing fruit as they are commercially replacing their heavy metal analogues. When searching for QD materials for use in LEDs, in solar cells or in imaging applications, the choice of material is currently somewhat limited (Figure 15).^[75,149] The most promising candidates in replacing classical QDs are InP/ZnS (ZnSe, ZnSeS) particles, and they have already found their way into many commercial products.^[148] However, they exhibit lower PLQYs, stemming from incomplete shells, strain between the shell and the core, and defects in the core material due to oxidation.^[47,149] While red and green LEDs with InP have been reported, with PLQYs of up to 95%, blue-emitting LEDs remain difficult to create. Further, while cadmium- and lead-containing nanoparticles are well studied and understood, heavy metal free ternary semiconductor nanocrystals suffer from understudied synthesis routes and optical properties.^[150] Here, multidimensional parameter scanning could be used to scan many combinations of, and reaction ratios between, material components, and could have a tremendous positive effect on advancing these nanoparticles.

Regarding perovskite nanoparticles, lead-free formulations currently fall short in performance when compared to LHPs. Typically, a replacement for lead consists of two or more elements, since it is difficult to find a substitute with same the size, electronic structure, and charge as lead. In such structures (e.g., silver bismuth perovskites), indirect bandgaps are common.^[76] Yang et al.^[151] recently reported a double perovskite structure involving silver, bismuth and indium (Cs₂AgIn_xBi_{1-x}Cl₆) with a direct bandgap above a threshold of $x = 0.75$ and a PLQE of 36.6%, which is close to typical LHP efficiencies. Direct bandgap nanocrystals show a higher absorption cross-section and higher PLQE than indirect nanocrystals due to phonon interactions that decrease charge carrier recom-

bination rates. In this respect, microfluidic multidimensional parameter screening could readily be used to scan for and fine-tune lead-free perovskite nanocrystals with direct bandgaps.

Instead of trying to recreate the efficiency of QDs and perovskites in lead- or cadmium-free analogues, assessing materials that are heavy metal free in their standard state is a promising alternative. In this regard, carbon and polymer-based nanoparticles have stimulated great interest. Graphene quantum dots (GQDs) and CDs are fully crystalline or partially amorphous carbon-based QDs with a high dependence on surface defects. Additionally, they show very high biodegradation rates and renal clearance.^[78,152] Precise engineering of CDs and GQDs is less developed than other nanoparticle types, however this process could be significantly accelerated by employing automated microfluidic platforms.^[78] Similarly, CPNs, despite their demonstrated performance in biological applications, still have much untapped potential.

5.2. Integrating Advanced Characterization Tools

While system-integrated absorption and PL detectors are compact, simple to operate, and yield important information, it is desirable to incorporate additional characterization tools to enrich the real-time analysis of nanoparticles during their synthesis. We now discuss two analysis techniques that may have an impact in the future of multidimensional parameter screening in microfluidic reactors for nanoparticles synthesis.

Photothermal spectroscopy (PS) is complementary to conventional absorption measurements. As previously discussed, reduced absorption signals due to short optical pathlengths has limited the efficacy of absorption detection in microfluidic systems. PS uses the photothermal effect during absorption to measure absorption cross sections.^[152] After photoexcitation of a nanoparticle, both radiative and nonradiative deactivation

will take place. While radiative decay yields emission of photons, nonradiative decay produces heat.^[21,52] The dissipated heat changes the refractive index of solvent in vicinity of the nanoparticle, and creates a thermal lens.^[153] A collinear probe beam can then be diffracted by the thermal lens, and used to extract a range of physical properties associated with the absorbing species. PS methods have been used in conjunction with microfluidic systems to detect single gold nanoparticles down to 5 nm in diameter and in fL volumes,^[154] and 10 nm particles in pL volumes.^[155,156] At a basic level, PS is a highly sensitive and background free absorption detection technique, that could replace absorption spectroscopy in microfluidic channels and engender a range of new analytical applications.

TEM allows determination of size, shape, crystal structure, and composition of a material in a thin, confined layer of solid or liquid. While conventional TEM is restricted to the analysis of solid/dry samples, liquid cell TEM (LC TEM) confines a thin layer of liquid between two windows of an electron transparent material, allowing visualization of structures in a liquid environment. These windows typically consist of nanometer-thick silicon nitride layers or graphene sheets of a few atomic layers.^[157] Graphene LCs are formed by entrapping a liquid bubble between two sheets of graphene. Despite their high resolution, graphene LCs are still limited in application by the small volume of entrapped liquid and short operational time frames (due to drying of the liquid when exposed to the electron beam).^[158,159] Silicon nitride windows are limited in terms of resolution due to scattering, but they are stable for longer periods, and most importantly offer the opportunity to perform in-flow measurements.^[157,160,161] For example, Nielsen et al.^[160] demonstrated LC TEM in a flow-cell to study the nucleation of CaCO₃. In this flow-cell, two syringes enter the LC through one inlet and exit through a single outlet, where the sample is collected. The nucleation of calcium carbonate was studied over a period of a few minutes at flow rates of between 0.2 and 10 $\mu\text{L min}^{-1}$. Although promising, performing LC TEM remains challenging. The measurement demands a high contrast TEM, and the use of acidic environments, which limits the materials that can be used.^[159,161–165] In LC TEM the electron beam is used to initiate nucleation and growth, or etching of nanoparticles. The influence of the electron beam on such processes is unknown and can limit the conclusions that may be drawn.^[166] Indeed, electron beams cause radiolysis in water, which gives rise to free radicals and changes in pH.^[167] The confinement of particles into a thin layer of liquid further has an influence on the diffusion of precursor species and movement of nanoparticles in solution, as shown by Wang et al.^[165] with a different liquid layer thickness resulting in different anisotropic growth.^[165,167] Consequently, it is not known how closely observed phenomena actually resemble processes occurring outside the LC environment. That said, the method does allow for a detailed study of nanoparticle nucleation, growth, and dissolution, and could, in unity with spectroscopic methods, unveil much additional structural and morphological information about single nanoparticles.

5.3. Learning from Organic Synthesis

To expand and optimize the range of QD materials, more advanced microfluidic platforms may be useful or even necessary. Concurrent advances in microfluidic reactors for

organic synthesis may provide inspiration here.^[168–170] Since traditional synthetic organic chemistry is not primarily focused on the manufacture of optically active products, but rather specific compositions with high yield, characterization units are typically quite different. For example, Sagmeister et al.^[168] presented a flow microreactor-based “lab of the future” with inline infrared spectroscopy (IR), inline nuclear magnetic resonance (NMR), online ultrahigh performance liquid chromatography (UPLC), an integrated mixing unit, and a heat exchanger. Moreover, Hsieh et al.^[169] demonstrated an interesting platform integrating multiparametric detection of refractive index variations, droplet velocity (and size), and encapsulated sample concentration. In addition to these complex platforms, Glotz and Kappe^[170] demonstrated an open-source USB photometer for use in flow, integrating an LED, detector, power supply, amplifier, and a control unit. This photometer could be connected to a flow cell consisting of a cross piece with optical fibers attached in one direction and a flow perpendicular to the light path. While the applications are different to those discussed herein, such platforms provide much inspiration for the development of photonic nanoparticle-oriented systems.

5.4. Leveraging Machine Learning

It has been suggested that the “fourth industrial revolution” that we are currently embarking upon will be defined by the combination of AI and big data.^[171] Indeed, the pervasive impact of this is already transforming the way that molecular and materials science research is performed.^[172,173] As previously discussed, high-throughput microfluidic experimentation is driving nanomaterial synthesis and characterization into the “big data” arena, fulfilling half of the above equation. The second half, then, requires the development and implementation of AI tools that keep pace with the data generation capacity, and allow us to unlock the inherent potential of cyber-physical systems in the field of microfluidics.

Machine learning, a subfield of AI, has recently gained much attention and some traction.^[174,175] It allows us to build mathematical models, based on training data, that can then be used to make predictions or perform tasks.^[176] The central model can be built by many different approaches, the most common being ANNs.^[145] Machine learning can yield sophisticated algorithms that are able to predict properties or extract hidden features in data based on the sheer weight of experience.

There is increasing sophistication and diversity in machine learning tools for generating, testing, and refining scientific models.^[173] A key feature of machine learning methods is the ability to feed an algorithm with a sufficient amount of quality training data to ensure the efficacy of the final model, and it is in this area that machine learning and microfluidic experimentation are perfectly matched.^[177,178] High-throughput microfluidics offers a solution to the challenges of data sparsity and data scarcity encountered in virtual synthesis parameter screening,^[179] and can far exceed the data-generation limitations of typical extended throughput approaches; for example, microwell plate-based syntheses.^[180]

Machine learning has been demonstrated to be a powerful tool for studying nanoparticle systems, both using purely

computational experimentation,^[181] and by combining large experimental data sets with machine learning-based analysis.^[180,182–187] We contend that the introduction of microfluidics into these studies will yield significant gains. Here, we can consider, forgetting practical challenges for the moment, three examples of how machine learning could be employed in microfluidic high-throughput screening experiments for photonic nanoparticle synthesis. First, machine learning could be used to maintain reactor stability during operation. If a reactor is to be run for hours to generate large data sets, it is imperative that it performs consistently, otherwise the resultant model will be skewed by both random and systematic errors. Unfortunately, due to factors such as microfluidic channel fouling, flow rate inconsistencies, and environmental fluctuations, it is hard to achieve absolute consistency. Recently, it has been demonstrated that machine learning can be used to achieve superhuman dynamic control of chip-based microfluidic experiments.^[188] Here, algorithms were developed to either maintain the position of an interface between two miscible flows within a microchannel under laminar flow, or to dynamically control the size of water-in-oil droplets in segmented flow, by variation of flow rates. Such ideas could be vital for ensuring reproducibility in longer-term microfluidic experimentation. Second, machine learning is adept at generating highly sophisticated models through extensive training with complex data sets from multidimensional scanning experiments. Here, large experiments with multiple inputs (e.g., precursor types/concentrations, surface ligand types/concentrations, solvents, and temperature), multiple inline, online, and offline analytical outputs (e.g., photoluminescence factors, absorption factors, particle size, and shape), and time course data, can yield rich data sets ripe for the supervised training of a machine learning algorithm. In this way, it becomes possible to learn the mechanisms that underlie the dataset, and extract features which are invisible to the human eye. Furthermore, data such as atomic characteristics of nanoparticle compositional elements (mass, oxidation states, etc.) and molecular characteristics of precursors and surface ligands (e.g., weight, bonding, and charge) could be included in the training data. Beyond reaction characterization, there are obvious benefits in being able to predict future materials based on extensive training experience of the algorithm.^[172] Finally, given a similarly complex set of inputs and outputs as described above, a machine learning algorithm trained with experimentally obtained data can be used to drive a reactor toward a specific desired product. The purpose need not be to thoroughly map a given parameter space and analyze complex input–output relationships, but simply to provide the optimal reaction formulation and protocol to yield the specific result. With repeated training for a variety of target outputs, and by feeding real-time data into the modeling,^[189,190] one could build a powerful microreactor system capable of extremely advanced targeted nanomaterials synthesis.

Although promising and potentially revolutionary, there is some caution to be maintained in machine learning. For example, it is important to consider potential error accumulation and loss of control that might compound through use.^[191] The function of a model in nanoparticle synthesis revolves around accurate prediction of nanoparticle properties in relation to the reaction parameters to form a highly accurate input–

output correlation.^[146] Since the accuracy of a trained model depends on the quality of the training, different training data or different models with the same training may yield different results. Additionally, overtraining a model with a specific data set may lead to errors and inaccuracies. This could result in, for example, errors in sensitivity or insensitivity toward certain parameters, and assuming incorrect relations between different parameters. Beyond errors in the model, problems could also arise due to sensitivity toward systematic or random errors in the data, which could be misleading and hard to disentangle in the final model, which would be exacerbated by the lack in transparency in some models, e.g., ANNs.^[192]

Although machine learning is a highly effective method in handling big data,^[175,193] other intelligent algorithms for reaction optimization have been reported, both independent of and in cooperation with machine learning. Gaussian process regression is a statistical approach used for modeling that has been successfully employed in microfluidic nanoparticle synthesis^[142,194] and has shown easy handling and successful reaction screening and optimization.^[195] Another attempt to solve complex optimization problems has been to use evolutionary computation (EC), which involves mimicry of evolutionary biology to develop a stochastic method for real parameter optimization, for example, the Covariance Matrix Adaptation Evolutionary Strategy (CMA-ES) has proven to be a good global optimizer.^[196,197] Genetic algorithms (GAs) mimic natural selection in the use of a populations, mutations, and successive generations, while measuring fitness and crossover within generations. GAs are applicable to real-world problems and have been shown to be quite robust.^[198] Further, the use of GAs has already been demonstrated for applications in reaction optimization, e.g., of methanol synthesis^[199] and fractional-order elements.^[200]

5.5. Widespread Usage and Impact

Although “smart” microfluidic platforms possess outstanding potential with regard to the synthesis of bespoke nanomaterials, their application and utility could be compromised by their (real or perceived) complexity, both in terms of hardware and software. In actual fact, microfluidic devices can be commercially purchased or fabricated according to unique requirements and easily integrated into a setup comprising commercially available parts. The complexity of a microfluidic platform merely depends on the requirements of the studied synthesis and necessary detection techniques. A fully automated platform need not involve the use of complex (machine learning) algorithms, but could simply incorporate a set of predefined parameters, that are consecutively scanned through. If more sophisticated system control is however desired, then an experienced personnel are of immense value in software design and optimization. Put simply, basic microfluidic reactors are broadly applicable and easy to assemble and operate. Conversely, the realization of more complex reaction systems will require some degree of specialized knowledge and/or multidisciplinary collaborations. Nevertheless, we contend that such hurdles are worth jumping!

When assembled, a microfluidic platform is able to synthesize a range of nanomaterials under a limited range of conditions. Although devices can be designed to withstand high pressures

and temperatures over extended periods of time, most microfluidic systems operate below 300 °C and provide for residence times up to tens of minutes. This limits the range of materials that can be synthesized. More extensive and harsh reactions, such as those needed for UCNPs, are far more challenging. Accordingly, the confrontation of unusual reaction conditions will necessarily involve creating more complex and robust reactors, and will undoubtedly be an area of much activity in the short to medium term. Finally, it is important to note that although integrated analytics offering real-time, inline and online characterization data are extremely powerful, they typically yield data on only the crude reaction product. However, it is well known that product purification is a vital component of the nanoparticle preparation process, and thus the development of integrated purification modules is an important frontier for the field, with some progress already being made in this direction.^[201]

6. Final Thoughts

In this review, we have detailed and discussed some of the most recent and impactful contributions to the field of microfluidic-based photonic nanoparticle synthesis, with a focus on automated multidimensional parameter scanning for materials characterization, optimization, and discovery. While the broad field of microfluidic nanomaterial synthesis is vibrant, systems reporting optimization via in situ optical characterization are less common, with the integration of smart control being even rarer.^[142,146] We predict that this situation will change drastically in the coming years, with many more studies demonstrating the incorporation of integrated analytics and sophisticated control. However, it should not be forgotten that even relatively simple systems that can be constructed and automated by non-experts can still have significant impact, and we hope that an increasing number of researchers in the nanomaterials community will adopt microfluidics as a basic tool. Although photoluminescent and plasmonic nanoparticles have already received much attention in a wide range of applications, there are still many undiscovered opportunities. In this respect, microfluidics is an ideal tool to explore new technologies and parametric landscapes for all kinds of nanomaterials.

This article is part of the Advanced Materials Technologies Hall of Fame article series, which recognizes the excellent contributions of leading researchers to the field of technology-related materials science.

Conflict of Interest

The authors declare no conflict of interest.

Keywords

machine learning, microfluidics, nanoparticles, photoluminescence, plasmonics

Received: January 24, 2020
Revised: March 12, 2020
Published online: May 10, 2020

- [1] A. P. Alivisatos, *Science* **1996**, 271, 933.
- [2] H. Weller, *Angew. Chem., Int. Ed. Engl.* **1993**, 32, 41.
- [3] O. S. Wolfbeis, *Chem. Soc. Rev.* **2015**, 44, 4743.
- [4] P. D. Howes, S. Rana, M. M. Stevens, *Chem. Soc. Rev.* **2014**, 43, 3835.
- [5] P. D. Howes, R. Chandrawati, M. M. Stevens, *Science* **2014**, 346, 1247390.
- [6] P. Devi, P. Rajput, A. Thakur, K. H. Kim, P. Kumar, *TrAC, Trends Anal. Chem.* **2019**, 114, 171.
- [7] S. M. Ng, M. Koneswaran, R. Narayanaswamy, *RSC Adv.* **2016**, 6, 21624.
- [8] S. Wen, J. Zhou, K. Zheng, A. Bednarkiewicz, X. Liu, D. Jin, *Nat. Commun.* **2018**, 9, 2415.
- [9] J. Li, J. Rao, K. Pu, *Biomaterials* **2018**, 155, 217.
- [10] B. Guo, J. Chen, N. Chen, E. Middha, S. Xu, Y. Pan, M. Wu, K. Li, C. Liu, B. Liu, *Adv. Mater.* **2019**, 31, 1808355.
- [11] B. Liu, *Conjugated Polymers for Biological and Biomedical Applications*, Wiley-VCH Verlag, Weinheim, Germany **2018**.
- [12] Y. Liu, P. Bhattarai, Z. Dai, X. Chen, *Chem. Soc. Rev.* **2019**, 48, 2053.
- [13] D. Tuncel, *Nanoscale Adv.* **2019**, 1, 19.
- [14] Y. Jiang, S. Y. Cho, M. Shim, *J. Mater. Chem. C* **2018**, 6, 2618.
- [15] K. Rakesh Tej Kumar, M. Ramakrishna, G. Durga Sukumar, *Int. J. Energy Res.* **2018**, 42, 2305.
- [16] M. A. Boles, D. Ling, T. Hyeon, D. V. Talapin, *Nat. Mater.* **2016**, 15, 141.
- [17] J. Liu, Y. Gu, Q. Wu, X. Wang, L. Zhao, A. deMello, W. Wen, R. Tong, X. Gong, *Crystals* **2019**, 9, 368.
- [18] I. Lignos, R. Maceiczky, A. J. deMello, *Acc. Chem. Res.* **2017**, 50, 1248.
- [19] L. J. Pan, J. W. Tu, H. T. Ma, Y. J. Yang, Z. Q. Tian, D. W. Pang, Z. L. Zhang, *Lab Chip* **2017**, 18, 41.
- [20] K. K. Kang, B. Lee, C. S. Lee, *J. Taiwan Inst. Chem. Eng.* **2019**, 98, 2.
- [21] R. M. Maceiczky, I. G. Lignos, A. J. deMello, *Curr. Opin. Chem. Eng.* **2015**, 8, 29.
- [22] A. M. Nightingale, J. C. deMello, *J. Mater. Chem.* **2010**, 20, 8454.
- [23] T. W. Phillips, I. G. Lignos, R. M. Maceiczky, A. J. deMello, J. C. deMello, *Lab Chip* **2014**, 14, 3172.
- [24] P. L. Saldanha, V. Lesnyak, L. Manna, *Nano Today* **2017**, 12, 46.
- [25] M. Thiele, J. Z. E. Soh, A. Knauer, D. Malsch, O. Stranik, R. Müller, A. Csáki, T. Henkel, J. M. Köhler, W. Fritzsche, *Chem. Eng. J.* **2016**, 288, 432.
- [26] C. Li, B. Ding, L. Zhang, K. Song, S. Tao, *J. Mater. Chem. C* **2019**, 7, 9167.
- [27] F. Fontana, J. P. Martins, G. Torrieri, H. A. Santos, *Adv. Mater. Technol.* **2019**, 4, 1800611.
- [28] A. M. Kaushik, K. Hsieh, T. H. Wang, *Wiley Interdiscip. Rev.: Nanomed. Nanobiotechnol.* **2018**, 10, 1522.
- [29] H. Song, J. D. Tice, R. F. Ismagilov, *Angew. Chem., Int. Ed.* **2003**, 42, 767.
- [30] B. K. H. Yen, A. Günther, M. A. Schmidt, K. F. Jensen, M. G. Bawendi, *Angew. Chem., Int. Ed.* **2005**, 44, 5447.
- [31] A. Suea-Ngam, P. D. Howes, M. Srisa-Art, A. J. deMello, *Chem. Commun.* **2019**, 55, 9895.
- [32] S. Duraiswamy, S. A. Khan, *Nano Lett.* **2010**, 10, 3757.
- [33] B. Herranz-Blanco, E. Ginestar, H. Zhang, J. Hirvonen, H. A. Santos, *Int. J. Pharm.* **2017**, 516, 100.
- [34] A. Toyota, H. Nakamura, H. Ozono, K. Yamashita, M. Uehara, H. Maeda, *J. Phys. Chem. C* **2010**, 114, 7527.
- [35] J. Baek, Y. Shen, I. Lignos, M. G. Bawendi, K. F. Jensen, *Angew. Chem., Int. Ed.* **2018**, 57, 10915.
- [36] M. P. Wolf, G. B. Salieb-Beugelaar, P. Hunziker, *Prog. Polym. Sci.* **2018**, 83, 97.
- [37] K. Ren, W. Dai, J. Zhou, J. Su, H. Wu, *Proc. Natl. Acad. Sci. USA* **2011**, 108, 8162.
- [38] M. Berenguel-Alonso, I. Ortiz-Gómez, B. Fernández, P. Couceiro, J. Alonso-Chamarro, L. F. Capitán-Vallvey, A. Salinas-Castillo, M. Puyol, *Sens. Actuators, B* **2019**, 296, 126613.

- [39] J. P. McMullen, K. F. Jensen, *Annu. Rev. Anal. Chem.* **2010**, *3*, 19.
- [40] A. deMello, *Lab Chip* **2002**, *2*, 31N.
- [41] Z. Mahmoodi, J. Mohammadnejad, S. Razavi Bazaz, A. Abouei Mehrizi, M. A. Ghiass, M. Saidijam, R. Dinarvand, M. Ebrahimi Warkiani, M. Soleimani, *Drug Delivery Transl. Res.* **2019**, *9*, 707.
- [42] T. Yang, J. Choo, S. Stavarakis, A. deMello, *Chem. - Eur. J.* **2018**, *24*, 12078.
- [43] I. Shestopalov, J. D. Tice, R. F. Ismagilov, *Lab Chip* **2004**, *4*, 316.
- [44] L. H. Hung, K. M. Choi, W. Y. Tseng, Y. C. Tan, K. J. Shea, A. P. Lee, *Lab Chip* **2006**, *6*, 174.
- [45] M. Lu, A. Ozcelik, C. L. Grigsby, Y. Zhao, F. Guo, K. W. Leong, T. J. Huang, *Nano Today* **2016**, *11*, 778.
- [46] D. Liu, H. Zhang, S. Cito, J. Fan, E. Mäkilä, J. Salonen, J. Hirvonen, T. M. Sikanen, D. A. Weitz, H. A. Santos, *Nano Lett.* **2017**, *17*, 606.
- [47] A. Vikram, V. Kumar, U. Ramesh, K. Balakrishnan, N. Oh, K. Deshpande, T. Ewers, P. Trefonas, M. Shim, P. J. A. Kenis, *Chem-NanoMat* **2018**, *4*, 943.
- [48] C. Wu, D. T. Chiu, *Angew. Chem., Int. Ed.* **2013**, *52*, 3086.
- [49] W. Liu, Y. Zhang, C. F. Wang, S. Chen, *RSC Adv.* **2015**, *5*, 107804.
- [50] T. Baby, Y. Liu, A. P. J. Middelberg, C. X. Zhao, *Chem. Eng. Sci.* **2017**, *169*, 128.
- [51] J. S. Sui, J. Y. Yan, D. Liu, K. Wang, G. S. Luo, *Small* **2020**, *16*, 1902828.
- [52] F. V. Ignatovich, L. Novotny, *Phys. Rev. Lett.* **2006**, *96*, 013901.
- [53] P. J. Worsfold, U. De Plymouth, R. Unido, E. A. G. Zagatto, U. D. S. Paulo, in *Encyclopedia of Analytical Science*, 3rd ed. (Eds: M. M. Worsfold, A. Townshend, C. Poole), Elsevier Ltd., Amsterdam **2017**, pp. 244–248.
- [54] L. E. Brus, *J. Chem. Phys.* **1984**, *80*, 4403.
- [55] R. L. Johnston, in *Metal Nanoparticles and Nanoalloys*, Vol. 3, (Eds: R. L. Johnston, J. Wilcoxon), Elsevier Science, Amsterdam **2012**, pp. 1–42.
- [56] E. M. Chan, M. A. Marcus, S. Fakra, M. ElNaggar, R. A. Mathies, A. Paul Alivisatos, *J. Phys. Chem. A* **2007**, *111*, 12210.
- [57] G. Tofghi, H. Lichtenberg, J. Pesek, T. L. Sheppard, W. Wang, L. Schöttner, G. Rinke, R. Dittmeyer, J. D. Grunwaldt, *React. Chem. Eng.* **2017**, *2*, 876.
- [58] G. Tofghi, X. Yu, H. Lichtenberg, D. E. Doronkin, W. Wang, C. Wöll, Y. Wang, J. D. Grunwaldt, *ACS Catal.* **2019**, *9*, 5462.
- [59] Z. H. Sun, H. Oyanagi, M. Uehara, H. Nakamura, K. Yamashita, A. Fukano, H. Maeda, *J. Phys. Chem. C* **2009**, *113*, 18608.
- [60] A. M. Karim, N. Al Hasan, S. Ivanov, S. Siefert, R. T. Kelly, N. G. Hallfors, A. Benavidez, L. Kovarik, A. Jenkins, R. E. Winans, A. K. Datye, *J. Phys. Chem. C* **2015**, *119*, 13257.
- [61] J. Timoshenko, Z. Duan, G. Henkelman, R. M. Crooks, A. I. Frenkel, *Annu. Rev. Anal. Chem.* **2019**, *12*, 501.
- [62] B. Abécassis, F. Testard, O. Spalla, P. Barboux, *Nano Lett.* **2007**, *7*, 50.
- [63] S. Krishnadasan, R. J. C. Brown, A. J. deMello, J. C. deMello, *Lab Chip* **2007**, *7*, 1434.
- [64] M. Karle, S. K. Vashist, R. Zengerle, F. von Stetten, *Anal. Chim. Acta* **2016**, *929*, 1.
- [65] N. X. Ca, N. T. Hien, N. T. Luyen, V. T. K. Lien, L. D. Thanh, P. V. Do, N. Q. Bau, T. T. Pham, *J. Alloys Compd.* **2019**, *787*, 823.
- [66] Y. Pu, F. Cai, D. Wang, J. X. Wang, J. F. Chen, *Ind. Eng. Chem. Res.* **2018**, *57*, 1790.
- [67] C. B. Murray, D. J. Norris, M. G. Bawendi, *J. Am. Chem. Soc.* **1993**, *115*, 8706.
- [68] A. Heuer-Jungemann, N. Feliu, I. Bakaimi, M. Hamaly, A. Alkilany, I. Chakraborty, A. Masood, M. F. Casula, A. Kostopoulou, E. Oh, K. Susumu, M. H. Stewart, I. L. Medintz, E. Stratakis, W. J. Parak, A. G. Kanaras, *Chem. Rev.* **2019**, *119*, 4819.
- [69] J. S. Lee, Y. H. Youn, I. K. Kwon, N. R. Ko, *J. Pharm. Invest.* **2018**, *48*, 209.
- [70] G. Halder, D. Ghosh, M. Y. Ali, A. Sahasrabudhe, S. Bhattacharyya, *Langmuir* **2018**, *34*, 10197.
- [71] D. A. Navarro, S. Banerjee, D. S. Aga, D. F. Watson, *J. Colloid Interface Sci.* **2010**, *348*, 119.
- [72] P. N. Wicinski, K. M. Metz, T. C. King Heiden, K. M. Louis, A. N. Mangham, R. J. Hamers, W. Heideman, R. E. Peterson, J. A. Pedersen, *Environ. Sci. Technol.* **2013**, *47*, 9132.
- [73] V. K. Sharma, T. J. McDonald, M. Sohn, G. A. K. Anquandah, M. Pettine, R. Zboril, *Chemosphere* **2017**, *188*, 403.
- [74] D. Hahm, D. Ko, B. G. Jeong, S. Jeong, J. Lim, W. K. Bae, C. Lee, K. Char, *J. Inf. Disp.* **2019**, *20*, 61.
- [75] Y. You, X. Tong, W. Wang, J. Sun, P. Yu, H. Ji, X. Niu, Z. M. Wang, *Adv. Sci.* **2019**, *6*, 1801967.
- [76] Y. Bekenstein, J. C. Dahl, J. Huang, W. T. Osowiecki, J. K. Swabeck, E. M. Chan, P. Yang, A. P. Alivisatos, *Nano Lett.* **2018**, *18*, 3502.
- [77] R. Wang, J. Wang, S. Tan, Y. Duan, Z. K. Wang, Y. Yang, *Trends Chem.* **2019**, *1*, 368.
- [78] Y. Yan, J. Gong, J. Chen, Z. Zeng, W. Huang, K. Pu, J. Liu, P. Chen, *Adv. Mater.* **2019**, *31*, 1808283.
- [79] G. Jia, Y. Pang, J. Ning, U. Banin, B. Ji, *Adv. Mater.* **2019**, *31*, 1900781.
- [80] S. Krishnadasan, J. Tovilla, R. Vilar, A. J. deMello, J. C. deMello, *J. Mater. Chem.* **2004**, *14*, 2655.
- [81] S. Yao, Y. Shu, Y. J. Yang, X. Yu, D. W. Pang, Z. L. Zhang, *Chem. Commun.* **2013**, *49*, 7114.
- [82] T. L. Sounart, P. A. Safer, J. A. Voigt, J. Hoyt, D. R. Tallant, C. M. Matzke, T. A. Michalske, *Lab Chip* **2007**, *7*, 908.
- [83] J. Pan, A. O. El-Ballouli, L. Rollny, O. Voznyy, V. M. Burlakov, A. Gorieli, E. H. Sargent, O. M. Bakr, *ACS Nano* **2013**, *7*, 10158.
- [84] S. Seibt, P. Mulvaney, S. Förster, *Colloids Surf., A* **2019**, *562*, 263.
- [85] S. V. Kershaw, N. M. Abdelazim, Y. Zhao, A. S. Susha, O. Zhovtiuk, W. Y. Teoh, A. L. Rogach, *Chem. Mater.* **2017**, *29*, 2756.
- [86] Y. Shu, P. Jiang, D. W. Pang, Z. L. Zhang, *Nanotechnology* **2015**, *26*, 275701.
- [87] M. Abolhasani, A. Oskooei, A. Klinkova, E. Kumacheva, A. Günther, *Lab Chip* **2014**, *14*, 2309.
- [88] M. Abolhasani, C. W. Coley, L. Xie, O. Chen, M. G. Bawendi, K. F. Jensen, *Chem. Mater.* **2015**, *27*, 6131.
- [89] J. Y. Rempel, M. G. Bawendi, K. F. Jensen, *J. Am. Chem. Soc.* **2009**, *131*, 4479.
- [90] R. M. Maceiczky, L. Bezing, A. J. deMello, *React. Chem. Eng.* **2016**, *1*, 261.
- [91] S. Lazzari, M. Abolhasani, K. F. Jensen, *React. Chem. Eng.* **2017**, *2*, 567.
- [92] Y. Shen, M. Abolhasani, Y. Chen, L. Xie, L. Yang, C. W. Coley, M. G. Bawendi, K. F. Jensen, *Angew. Chemie., Int. Ed.* **2017**, *56*, 16333.
- [93] J. Yue, F. H. Falke, J. C. Schouten, T. A. Nijhuis, *Lab Chip* **2013**, *13*, 4855.
- [94] S. Lazzari, P. M. Theiler, Y. Shen, C. W. Coley, A. Stemmer, K. F. Jensen, *Langmuir* **2018**, *34*, 3307.
- [95] B. Swain, M. H. Hong, L. Kang, B. S. Kim, N. H. Kim, C. G. Lee, *Chem. Eng. J.* **2017**, *308*, 311.
- [96] M. V. Kovalenko, L. Protesescu, M. I. Bodnarchuk, *Science* **2017**, *358*, 745.
- [97] H. Huang, M. I. Bodnarchuk, S. V. Kershaw, M. V. Kovalenko, A. L. Rogach, *ACS Energy Lett.* **2017**, *2*, 2071.
- [98] K. Niu, Y. Li, R. Bai, Y. Qu, Y. Song, *J. Mater. Chem. B* **2017**, *5*, 5145.
- [99] S. T. Ochsenein, F. Krieg, Y. Shynkarenko, G. Rainò, M. V. Kovalenko, *ACS Appl. Mater. Interfaces* **2019**, *11*, 21655.
- [100] M. V. Kovalenko, L. Manna, A. Cabot, Z. Hens, D. V. Talapin, C. R. Kagan, V. I. Klimov, A. L. Rogach, P. Reiss, D. J. Milliron, P. Guyot-Sionnest, G. Konstantatos, W. J. Parak, T. Hyeon, B. A. Korgel, C. B. Murray, W. Heiss, *ACS Nano* **2015**, *9*, 1012.
- [101] Z. Li, Q. Hu, Z. Tan, Y. Yang, M. Leng, X. Liu, C. Ge, G. Niu, J. Tang, *ACS Appl. Mater. Interfaces* **2018**, *10*, 43915.
- [102] G. Almeida, L. Goldoni, Q. Akkerman, Z. Dang, A. H. Khan, S. Marras, I. Moreels, L. Manna, *ACS Nano* **2018**, *12*, 1704.

- [103] W. Lv, L. Li, M. Xu, J. Hong, X. Tang, L. Xu, Y. Wu, R. Zhu, R. Chen, W. Huang, *Adv. Mater.* **2019**, *31*, 1900682.
- [104] I. Lignos, V. Morad, Y. Shynkarenko, C. Bernasconi, R. M. Maceczyk, L. Protesescu, F. Bertolotti, S. Kumar, S. T. Ochsenein, N. Masciocchi, A. Guagliardi, C. J. Shih, M. I. Bodnarchuk, A. J. deMello, M. V. Kovalenko, *ACS Nano* **2018**, *12*, 5504.
- [105] L. Protesescu, S. Yakunin, M. I. Bodnarchuk, F. Krieg, R. Caputo, C. H. Hendon, R. X. Yang, A. Walsh, M. V. Kovalenko, *Nano Lett.* **2015**, *15*, 3692.
- [106] I. Lignos, L. Protesescu, D. B. Emiroglu, R. Maceczyk, S. Schneider, M. V. Kovalenko, A. J. deMello, *Nano Lett.* **2018**, *18*, 1246.
- [107] I. Lignos, R. M. Maceczyk, M. V. Kovalenko, S. Stavrakis, *Chem. Mater.* **2019**, *32*, 27.
- [108] R. W. Epps, K. C. Felton, C. W. Coley, M. Abolhasani, *Lab Chip* **2017**, *17*, 4040.
- [109] K. Abdel-Latif, R. W. Epps, C. B. Kerr, C. M. Papa, F. N. Castellano, M. Abolhasani, *Adv. Funct. Mater.* **2019**, *29*, 1900712.
- [110] J. Yu, Y. Rong, C. T. Kuo, X. H. Zhou, D. T. Chiu, *Anal. Chem.* **2017**, *89*, 42.
- [111] K. Sun, Y. Yang, H. Zhou, S. Yin, W. Qin, J. Yu, D. T. Chiu, Z. Yuan, X. Zhang, C. Wu, *ACS Nano* **2018**, *12*, 5176.
- [112] R. Couto, S. Chambon, C. Aymonier, E. Mignard, B. Pavageau, A. Erriguible, S. Marre, *Chem. Commun.* **2015**, *51*, 1008.
- [113] T. M. Swager, *Macromolecules* **2017**, *50*, 4867.
- [114] J. G. Ibanez, M. E. Rincón, S. Gutierrez-Granados, M. Chahma, O. A. Jaramillo-Quintero, B. A. Frontana-Urbe, *Chem. Rev.* **2018**, *118*, 4731.
- [115] X. Z. Lim, *Nature* **2016**, *531*, 26.
- [116] A. J. C. Kuehne, *Adv. Biosyst.* **2017**, *1*, 1700100.
- [117] Y. Jiang, J. McNeill, *Chem. Rev.* **2017**, *117*, 838.
- [118] J. Tao, S. F. Chow, Y. Zheng, *Acta Pharm. Sin. B* **2019**, *9*, 4.
- [119] F. Kong, X. L. Wu, G. S. Huang, R. K. Yuan, P. K. Chu, *Thin Solid Films* **2008**, *516*, 6287.
- [120] B. Guo, E. Middha, B. Liu, *ACS Nano* **2019**, *13*, 2675.
- [121] D. Liu, S. Cito, Y. Zhang, C. F. Wang, T. M. Sikanen, H. A. Santos, *Adv. Mater.* **2015**, *27*, 2298.
- [122] C. Martins, F. Araújo, M. J. Gomes, C. Fernandes, R. Nunes, W. Li, H. A. Santos, F. Borges, B. Sarmiento, *Eur. J. Pharm. Biopharm.* **2019**, *138*, 111.
- [123] A. J. C. Kuehne, D. A. Weitz, *Chem. Commun.* **2011**, *47*, 12379.
- [124] T. F. Abelha, T. W. Phillips, J. H. Bannock, A. M. Nightingale, C. A. Dreiss, E. Kemal, L. Urbano, J. C. deMello, M. Green, L. A. Dailey, *Nanoscale* **2017**, *9*, 2009.
- [125] F. Schütze, B. Stempfle, C. Jüngst, D. Wöll, A. Zumbusch, S. Mecking, *Chem. Commun.* **2012**, *48*, 2104.
- [126] S. R. Jung, R. Han, W. Sun, Y. Jiang, B. S. Fujimoto, J. Yu, C. T. Kuo, Y. Rong, X. H. Zhou, D. T. Chiu, *Anal. Chem.* **2018**, *90*, 6089.
- [127] J. Zhu, X. Bai, X. Chen, H. Shao, Y. Zhai, G. Pan, H. Zhang, E. V. Ushakova, Y. Zhang, H. Song, A. L. Rogach, *Adv. Opt. Mater.* **2019**, *7*, 1801599.
- [128] Y. Lu, L. Zhang, H. Lin, *Chem. - Eur. J.* **2014**, *20*, 4246.
- [129] K. Malecha, *Int. J. Appl. Ceram. Technol.* **2016**, *13*, 69.
- [130] M. Thiele, A. Knauer, D. Malsch, A. Csáki, T. Henkel, J. M. Köhler, W. Fritzsche, *Lab Chip* **2017**, *17*, 1487.
- [131] M. H. Jazayeri, H. Amani, A. A. Pourfatollah, H. Pazoki-Toroudi, B. Sedighimoghaddam, *Sens. Bio-Sens. Res.* **2016**, *9*, 17.
- [132] R. Jin, C. Zeng, M. Zhou, Y. Chen, *Chem. Rev.* **2016**, *116*, 10346.
- [133] D. Bain, S. Maity, A. Patra, *Phys. Chem. Chem. Phys.* **2019**, *21*, 5863.
- [134] A. Knauer, A. Eisenhardt, S. Krischok, J. M. Koehler, *Nanoscale* **2014**, *6*, 5230.
- [135] S. Merken, M. Vakili, A. Sánchez-Iglesias, L. Litti, Y. Gao, P. V. Gwozd, L. Sharpnack, R. H. Blick, L. M. Liz-Marzán, M. Grzelczak, M. Trebbin, *ACS Nano* **2019**, *13*, 6596.
- [136] J. Timoshenko, Z. Duan, G. Henkelman, R. M. Crooks, A. I. Frenkel, *Annu. Rev. Anal. Chem.* **2019**, *12*, 501.
- [137] B. Gu, Q. Zhang, *Adv. Sci.* **2018**, *5*, 1700609.
- [138] F. Wang, R. Deng, J. Wang, Q. Wang, Y. Han, H. Zhu, X. Chen, X. Liu, *Nat. Mater.* **2011**, *10*, 968.
- [139] D. Liu, Y. Jing, K. Wang, Y. Wang, G. Luo, *Nanoscale* **2019**, *11*, 8363.
- [140] F. Wang, R. Deng, X. Liu, *Nat. Protoc.* **2014**, *9*, 1634.
- [141] W. Huyer, A. Neumaier, *ACM Trans. Math. Software* **2008**, *35*, 9.
- [142] L. Bezinge, R. M. Maceczyk, I. Lignos, M. V. Kovalenko, A. J. deMello, *ACS Appl. Mater. Interfaces* **2018**, *10*, 18869.
- [143] R. M. Maceczyk, A. J. deMello, *J. Phys. Chem. C* **2014**, *118*, 20026.
- [144] C. B. Kerr, R. W. Epps, M. Abolhasani, *Lab Chip* **2019**, *19*, 2107.
- [145] Y. Bengio, A. Courville, P. Vincent, *IEEE Trans. Pattern Anal. Mach. Intell.* **2013**, *35*, 1798.
- [146] Y. Orimoto, K. Watanabe, K. Yamashita, M. Uehara, H. Nakamura, T. Furuya, H. Maeda, *J. Phys. Chem. C* **2012**, *116*, 17885.
- [147] K. Watanabe, Y. Orimoto, K. Nagano, K. Yamashita, M. Uehara, H. Nakamura, T. Furuya, H. Maeda, *Chem. Eng. Sci.* **2012**, *75*, 292.
- [148] Samsung, "Der Umwelt zuliebe: Samsung QLED TV ohne Cadmium", <https://www.samsung.com/at/discover/der-umwelt-zuliebe-samsung-qled-tv-ohne-cadmium/> (accessed: November 2019).
- [149] C. Ippen, W. Guo, D. Zehnder, D. Kim, J. Manders, D. Barrera, B. Newmeyer, D. Hamilton, C. Wang, C. Hotz, R. Ma, J. K. Bin, B. G. Kim, K. N. Kim, K. K. Jang, J. Park, T. Lee, W. Y. Kim, J. H. Lee, *J. Soc. Inf. Disp.* **2019**, *27*, 338.
- [150] A. C. Berends, M. J. J. Mangnus, C. Xia, F. T. Rabouw, C. De, M. Donega, *J. Phys. Chem. Lett.* **2019**, *10*, 1600.
- [151] B. Yang, X. Mao, F. Hong, W. Meng, Y. Tang, X. Xia, S. Yang, W. Deng, K. Han, *J. Am. Chem. Soc.* **2018**, *140*, 17001.
- [152] H. Soo Choi, W. Liu, P. Misra, E. Tanaka, J. P. Zimmer, B. Itty Ipe, M. G. Bawendi, J. V. Frangioni, *Nat. Biotechnol.* **2007**, *25*, 1165.
- [153] M. A. Lima, A. M. Olaizola, G. L. Gamboa, M. P. P. de Castro, M. S. Stel, *J. Nanopart. Res.* **2019**, *21*, 118.
- [154] H. Shimizu, K. Mawatari, T. Kitamori, *Anal. Chem.* **2009**, *81*, 9802.
- [155] M. Selmke, A. Heber, M. Braun, F. Cichos, *Appl. Phys. Lett.* **2014**, *105*, 013511.
- [156] R. Maceczyk, H. Shimizu, D. Müller, T. Kitamori, A. deMello, *Anal. Chem.* **2017**, *89*, 1994.
- [157] F. M. Ross, *Science* **2015**, *350*, aaa9886.
- [158] X. Ye, M. R. Jones, L. B. Frechette, Q. Chen, A. S. Powers, P. Ercius, G. Dunn, G. M. Rotskoff, S. C. Nguyen, V. P. Adiga, A. Zettl, E. Rabani, P. L. Geissler, A. P. Alivisatos, *Science* **2016**, *354*, 874.
- [159] M. R. Hauwiler, J. C. Ondry, C. M. Chan, P. Khandekar, J. Yu, A. P. Alivisatos, *J. Am. Chem. Soc.* **2019**, *141*, 4428.
- [160] M. H. Nielsen, S. Aloni, J. J. De Yoreo, *Science* **2014**, *345*, 1158.
- [161] B. H. Kim, J. Yang, D. Lee, B. K. Choi, T. Hyeon, J. Park, *Adv. Mater.* **2018**, *30*, 1703316.
- [162] J. Li, J. Chen, H. Wang, N. Chen, Z. Wang, L. Guo, F. L. Deepak, *Adv. Sci.* **2018**, *5*, 1700992.
- [163] C. Zhu, S. Liang, E. Song, Y. Zhou, W. Wang, F. Shan, Y. Shi, C. Hao, K. Yin, T. Zhang, J. Liu, H. Zheng, L. Sun, *Nat. Commun.* **2018**, *9*, 421.
- [164] J. Park, H. Elmlund, P. Ercius, J. M. Yuk, D. T. Limmer, Q. Chen, K. Kim, S. H. Han, D. A. Weitz, A. Zettl, A. P. Alivisatos, *Science* **2015**, *349*, 290.
- [165] S. T. Wang, Y. Lin, M. H. Nielsen, C. Y. Song, M. R. Thomas, C. D. Spicer, R. Kröger, P. Ercius, S. Aloni, M. M. Stevens, *Nanoscale* **2019**, *11*, 16801.
- [166] S. F. Tan, S. W. Chee, G. Lin, U. Mirsaidov, *Acc. Chem. Res.* **2017**, *50*, 1303.
- [167] N. M. Schneider, M. M. Norton, B. J. Mendel, J. M. Grogan, F. M. Ross, H. H. Bau, *J. Phys. Chem. C* **2014**, *118*, 22373.
- [168] P. Sagmeister, J. D. Williams, C. A. Hone, C. O. Kappe, *React. Chem. Eng.* **2019**, *4*, 1571.
- [169] Y. W. Hsieh, A. B. Wang, X. Y. Lu, L. A. Wang, *Sens. Actuators, B* **2016**, *237*, 841.
- [170] G. Glotz, C. O. Kappe, *React. Chem. Eng.* **2018**, *3*, 478.

- [171] K. Schwab, *The Fourth Industrial Revolution*, Penguin Books, London **2017**.
- [172] B. Sanchez-Lengeling, A. Aspuru-Guzik, *Science* **2018**, *361*, 360.
- [173] K. T. Butler, D. W. Davies, H. Cartwright, O. Isayev, A. Walsh, *Nature* **2018**, *559*, 547.
- [174] M. I. Jordan, T. M. Mitchell, *Science* **2015**, *349*, 255.
- [175] R. Ramprasad, R. Batra, G. Pilania, A. Mannodi-Kanakithodi, C. Kim, *npj Comput. Mater.* **2017**, *3*, 54.
- [176] D. J. C. MacKay, *Information Theory, Inference, and Learning Algorithms*, Cambridge University Press, Cambridge **2003**.
- [177] J. Riordon, D. Sovilj, S. Sanner, D. Sinton, E. W. K. Young, *Trends Biotechnol.* **2019**, *37*, 310.
- [178] D. M. Camacho, K. M. Collins, R. K. Powers, J. C. Costello, J. J. Collins, *Cell* **2018**, *173*, 1581.
- [179] E. Kim, K. Huang, S. Jegelka, E. Olivetti, *npj Comput. Mater.* **2017**, *3*, 53.
- [180] G. Yamankurt, E. J. Berns, A. Xue, A. Lee, N. Bagheri, M. Mrksich, C. A. Mirkin, *Nat. Biomed. Eng.* **2019**, *3*, 318.
- [181] B. Sun, H. Barron, G. Opletal, A. S. Barnard, *J. Phys. Chem. C* **2018**, *122*, 28085.
- [182] S. M. Copp, A. Gorovits, S. M. Swasey, S. Gudibandi, P. Bogdanov, E. G. Gwinn, *ACS Nano* **2018**, *12*, 8240.
- [183] N. Saadatkah, S. Aghamiri, M. R. Talaie, G. S. Patience, *CrystEngComm* **2018**, *20*, 7590.
- [184] E. J. Braham, J. Cho, K. M. Forlano, D. F. Watson, R. Arròyave, S. Banerjee, *Chem. Mater.* **2019**, *31*, 3281.
- [185] R. Yuan, Y. Tian, D. Xue, D. Xue, Y. Zhou, X. Ding, J. Sun, T. Lookman, *Adv. Sci.* **2019**, *6*, 1901395.
- [186] A. Mikolajczyk, N. Sizochenko, E. Mulkiewicz, A. Malankowska, B. Rasulev, T. Puzyn, *Nanoscale* **2019**, *11*, 11808.
- [187] O. Voznyy, L. Levina, J. Z. Fan, M. Askerka, A. Jain, M.-J. Choi, O. Ouellette, P. Todorović, L. K. Sagar, E. H. Sargent, *ACS Nano* **2019**, *13*, 11122.
- [188] O. J. Dressler, P. D. Howes, J. Choo, A. J. deMello, *ACS Omega* **2018**, *3*, 10084.
- [189] S. V. Kalinin, B. G. Sumpter, R. K. Archibald, *Nat. Mater.* **2015**, *14*, 973.
- [190] B. J. Reizman, K. F. Jensen, *Acc. Chem. Res.* **2016**, *49*, 1786.
- [191] G. Schneider, *Nat. Rev. Drug Discovery* **2018**, *17*, 97.
- [192] S. Webb, *Nature* **2018**, *554*, 555.
- [193] Z. Zhou, X. Li, R. N. Zare, *ACS Cent. Sci.* **2017**, *3*, 1337.
- [194] B. Wang, T. Chen, *Chemom. Intell. Lab. Syst.* **2015**, *142*, 159.
- [195] K. Omata, *Ind. Eng. Chem. Res.* **2011**, *50*, 10948.
- [196] S. Ghosh, S. Das, S. Roy, S. K. Minhazul Islam, P. N. Suganthan, *Inf. Sci.* **2012**, *182*, 199.
- [197] N. Hansen, in *Towards a New Evolutionary Computation*, Vol. 192 (Eds: J. A. Lozano, P. Larrañaga, I. Inza, E. Bengoetxea), Springer-Verlag, Berlin, Heidelberg **2006**, pp. 75–95.
- [198] C. García-Martínez, F. J. Rodríguez, M. Lozano, *Handb. Heuristics* **2018**, *1–2*, 431.
- [199] H. Kordabadi, A. Jahanmiri, *Chem. Eng. J.* **2005**, *108*, 249.
- [200] A. Kartci, A. Agambayev, M. Farhat, N. Herencsar, L. Brancik, H. Bagci, K. N. Salama, *IEEE Access* **2019**, *7*, 80233.
- [201] G. Niu, L. Zhang, A. Ruditskiy, L. Wang, Y. Xia, *Nano Lett.* **2018**, *18*, 3879.
- [202] S. Merkens, M. Vakili, A. Sanchez-Iglesias, L. Litti, Y. Gao, P. V. Gwozdz, L. Sharpnack, R. H. Blick, L. M. Liz-Marzan, M. Grzelczak, M. Trebbin, *ACS Nano* **2019**, *13*, 6596.
- [203] M. Saliba, J. P. Correa-Baena, M. Grätzel, A. Hagfeldt, A. Abate, *Angew. Chem., Int. Ed.* **2018**, *57*, 2554.